



HAL
open science

Recycling of nitrogen and light noble gases in the Central American subduction zone: constraints from 15 N 15 N

Jabrane Labidi, E.D. Young, T.P. Fischer, P.H. Barry, C.J. Ballentine, J.M.
de Moor

► **To cite this version:**

Jabrane Labidi, E.D. Young, T.P. Fischer, P.H. Barry, C.J. Ballentine, et al.. Recycling of nitrogen and light noble gases in the Central American subduction zone: constraints from 15 N 15 N. Earth and Planetary Science Letters, 2021, 571, pp.117112. 10.1016/j.epsl.2021.117112 . hal-03325181

HAL Id: hal-03325181

<https://hal.science/hal-03325181v1>

Submitted on 24 Aug 2021

HAL is a multi-disciplinary open access archive for the deposit and dissemination of scientific research documents, whether they are published or not. The documents may come from teaching and research institutions in France or abroad, or from public or private research centers.

L'archive ouverte pluridisciplinaire **HAL**, est destinée au dépôt et à la diffusion de documents scientifiques de niveau recherche, publiés ou non, émanant des établissements d'enseignement et de recherche français ou étrangers, des laboratoires publics ou privés.

1 **Recycling of nitrogen and light noble gases in the Central American subduction zone: constraints from**

2 $^{15}\text{N}^{15}\text{N}$

3 J. Labidi¹, E.D. Young², T.P. Fischer³, P.H. Barry⁴, C.J. Ballentine⁵, J.M. de Moor^{3,6}

4

5 ¹ Université de Paris, Institut de physique du globe de Paris, CNRS, Paris, France

6 ² Department of Earth, Planetary, and Space Sciences, UCLA, Los Angeles, CA, USA.

7 ³ Department of Earth and Planetary Sciences, University of New Mexico, Albuquerque, NM 87131-1116, USA

8 ⁴ Marine Chemistry and Geochemistry Department, Woods Hole Oceanographic Institution, Woods Hole MA 02543

9 USA

10 ⁵ Department of Earth Sciences, University of Oxford, OX1 3AN, UK

11 ⁶ Observatorio Volcanológico y Sismológico de Costa Rica (OVSICORI), Universidad Nacional, Costa Rica

12

13

14 **Abstract**

15 How much nitrogen and light noble gases are recycled in modern subduction zones is

16 unclear. Fumaroles act as a means for passive degassing in arcs. They receive variable

17 contributions of volatiles from arc magmas, themselves sourced from the mantle wedge.

18 The gas compositions reflect the extent of volatile enrichment in sub-arc mantle sources

19 and constrain slab dehydration. However, contributions from atmospheric components in

20 fumaroles are unavoidable. For N₂, neon and argon, the atmospheric components are

21 challenging to discern from slab-derived components. Here, we report $^{15}\text{N}^{15}\text{N}$

22 measurements from eight fumaroles and seven bubbling springs, along the Central

23 American arc. Our new $^{15}\text{N}^{15}\text{N}$ data are coupled with noble gases measurements and show

24 that air-derived components in volcanic gas discharges can easily be underestimated, in

25 both fumaroles and springs, using conventional stable isotope or noble gases methods. We

26 show that, in the absence of $^{15}\text{N}^{15}\text{N}$ data, previously used tracers for air (e.g., $\delta^{15}\text{N}$, N_2/Ar ,
27 N_2/He , among others) may lead to erroneous conclusions regarding the origin of volatiles
28 in mixed gases. In contrast, $^{15}\text{N}^{15}\text{N}$ data provide quantitative constraints on the nature and
29 contributions of both atmospheric and magmatic components. Most springs are heavily
30 dominated by air-derived N_2 , while fumaroles show substantial contributions of volcanic
31 endmembers. Based on the fumarole data, we show that magma sources beneath the
32 central American arc are enriched in all volatiles relative to ^3He , by two to three orders of
33 magnitude compared to the MORB source. We use new $^{15}\text{N}^{15}\text{N}$ data to obtain source
34 $\text{N}_2/{}^3\text{He}$, ${}^3\text{He}/{}^{36}\text{Ar}$ and ${}^3\text{He}/{}^{22}\text{Ne}$ ratios which we then use to compute volcanic N_2 , Ar and Ne
35 degassing fluxes. Using this approach, we show that outgassing fluxes appear to match
36 subduction fluxes in the Central America subduction zone. We determine an N_2 outgassing
37 flux of between 4.0×10^8 and 1.0×10^9 mol N_2/y , comparable to the subduction flux of $5.7 \times$
38 10^8 mol N_2/yr determined previously. We obtain a similar conclusion for ${}^{22}\text{Ne}$ and ${}^{36}\text{Ar}$.
39 Overall, the volatile fluxes in the central American subduction zone no longer seem to
40 require net transfer of N_2 , Ar, and Ne, to the deep mantle.

41

42 **1. Introduction**

43 The origin of volatiles emitted from convergent margins provides fundamental
44 constraints on how plate tectonics redistributes volatiles between terrestrial reservoirs
45 (Bekaert et al., 2020; Hilton et al., 2002; Plank et al., 2013). The nitrogen cycle is under-
46 constrained, partly because quantifying degassing N_2 fluxes in arcs is challenging. For
47 instance, basalt glasses are virtually absent in subduction zones, impeding quantification of
48 nitrogen elemental abundances in the underlying mantle wedge. The systematic study of

49 metamorphic rocks has suggested nitrogen is quantitatively retained within minerals in
50 downgoing slabs (Bebout et al., 2013; Busigny et al., 2003). The latter is based on the
51 composition of rocks from the European alps, where sediments underwent metamorphism
52 in a cold subduction zone (630 °C at 100 km, Busigny et al., 2003). In those rocks, nitrogen
53 is hosted in the structures of clay minerals including micas and illites, as NH_4^+ substituting
54 for potassium (Bebout et al., 1992, Busigny et al., 2003; Nieder et al., 2011). Experimental
55 work confirms that the fluid/rock nitrogen partition coefficient in a cold P-T pathway is in
56 favor of N retention in minerals (Jackson et al., 2021). However, under warmer conditions,
57 fluid/rock partitioning favors N accumulation in fluids, potentially limiting nitrogen
58 subduction to the mantle (Jackson et al., 2021). Subduction temperature gradients were
59 likely steeper in most of the Proterozoic and Archean (Martin and Moyen, 2002). Therefore,
60 it is unclear how modern fluxes determined in cold subduction zones should be
61 extrapolated back into deep time.

62 The Central American Volcanic Arc (CAVA) is relatively well-characterized with
63 evidence for sedimentary and igneous components from the slab variably contributing to
64 mantle sources across the arc (Patino et al., 2000). It is a “warm” subduction zone, with
65 predicted slab interface temperatures of ~ 800 °C at 100 km depth beneath Costa Rica
66 (Peacock et al., 2005), resulting in sporadic slab melting (Hoernle et al., 2008). Thus, it may
67 be considered an analog for subduction zones at a time when subduction temperature
68 gradients were steeper. In Central America, metamorphic rocks cannot be used to constrain
69 net subduction fluxes because no section of metasediments having undergone the
70 subduction P-T pathway is known to occur in the geological record. Instead, net subduction
71 fluxes of volatiles are estimated from comparing their concentrations and isotopic

72 compositions in the offshore altered oceanic crust (Li and Bebout, 2005, Busigny et al.,
73 2019) with their concentrations and isotopic compositions in arc fumaroles that represent
74 volcanic outgassing fluxes. This mass balance calculation can be hampered by ubiquitous
75 infiltration of air into most fumaroles, as evidenced by noble gases systematics: although
76 fumaroles typically show mantle-like helium isotope ratios, neon and argon budgets are
77 overwhelmed by atmospheric components (Hilton et al., 2002; Snyder et al., 2003). This is
78 also a problem for nitrogen. Historically, SO_2/N_2 ratios from fumaroles and the overall SO_2
79 outgassing flux has been used to determine a total N_2 volcanic outgassing flux for the
80 central American arc, yielding a value of 1.7×10^9 mol N_2/yr , or 3.4×10^9 mol N/yr (Hilton
81 et al., 2002, Fischer et al., 2002). This is comparable to an estimate of the central American
82 subduction nitrogen flux of $\sim 1.1 \times 10^9$ mol N/yr (equivalent to $\sim 5.7 \times 10^8$ mol N_2/yr) from
83 Busigny et al. (2019). These flux estimates are given with no uncertainties, but they appear
84 comparable within a factor of 2. Taken at face value, this would support inefficient N
85 recycling from the surface to the deep mantle. However, fumaroles incorporate air-derived
86 N_2 , after the infiltration of meteoric water within subsurface hydrothermal systems and/or
87 because of sampling techniques (Fischer et al., 2002). Thus, the outgassing N_2 fluxes based
88 on raw N_2/SO_2 ratios in fumaroles are overestimates of the outgassing N_2 flux. As a remedy,
89 the volcanic fraction of N_2 in fumaroles was quantified on the basis of N_2/Ar ratios: air-
90 saturated waters have a known N_2/Ar ratio of ~ 40 at STP but most hydrothermal gases in
91 the CAVA have ratios > 80 (Hilton et al., 2002; Fischer et al., 2002, Elkins et al., 2006,
92 Snyder et al., 2003; Zimmer et al., 2004). The N_2 amount in excess of air-saturated water,
93 termed N_2^* , was suggested to reflect the volcanic N_2 fraction (Hilton et al., 2002, Fischer et
94 al., 2002). A volcanic nitrogen degassing flux of 2.9×10^8 mol N_2/year was estimated for the

95 central American arc (Fischer et al., 2002). This degassing flux estimate is lower by a factor
96 of 2 than the subduction nitrogen flux of $\sim 5.7 \times 10^8$ mol N₂/year (or $\sim 1.1 \times 10^9$ mol N/yr),
97 suggesting N₂ sequestration into the deep mantle by subduction, even in a warm
98 subduction zone (Busigny et al., 2019; Li and Bebout, 2005).

99 Here, we take a new approach to constrain the origin of N₂ as well as light noble gases
100 in CAVA fumaroles and springs. We use the newly-developed ¹⁵N¹⁵N tracer of atmospheric
101 contamination (Labidi et al., 2020; Yeung et al., 2017; Young et al., 2016). Specifically, we
102 use Δ_{30} , the ¹⁵N¹⁵N concentration relative to a random distribution of ¹⁴N and ¹⁵N atoms
103 among N₂ molecules, as a tracer of surficial atmospheric contamination. The Δ_{30} tracer is
104 defined as $\Delta_{30} = {}^{30}\text{R}/({}^{15}\text{R})^2 - 1$ (‰), where ${}^{30}\text{R} = {}^{15}\text{N}^{15}\text{N}/{}^{14}\text{N}^{14}\text{N}$ and ${}^{15}\text{R} = {}^{15}\text{N}/{}^{14}\text{N}$ for the gas
105 of interest. At relevant temperatures ranging from 200 to 1000 °C, equilibrium among N₂
106 isotopologues results in Δ_{30} values from 0.5 to 0.1‰, respectively (Yeung et al., 2017). This
107 applies for any magmatic and crustal N₂, whether it is mantle-derived, inherited from the
108 slab, or shallow crustal reservoirs (Labidi et al., 2020). In contrast, air has a pronounced
109 disequilibrium ¹⁵N¹⁵N enrichment, leading to an atmospheric Δ_{30} value of 19.1 ± 0.3 ‰ (2σ)
110 (Yeung et al., 2017). We make use of this disequilibrium as a tracer for air contributions in
111 natural fluids and identify the compositions of mantle sources for N₂ and light noble gases
112 for 15 fumaroles and gases bubbling from springs in Costa Rica, Panama, Nicaragua, and El
113 Salvador. Our ¹⁵N¹⁵N data allows determination of the N₂/³He, ³He/³⁶Ar and ³He/²²Ne
114 ratios for the CAVA mantle sources. Using an updated ³He outgassing flux for the region, we
115 provide a new range of estimates for the N₂ outgassing flux along the Central American arc.
116 Our result has implications for the net subduction flux of nitrogen, suggesting that the net
117 sequestration of nitrogen to the mantle is within error of zero.

118

119 **2. Geological context and samples**

120 The CAVA results from the eastward subduction of the Cocos Plate beneath the
121 Caribbean Plate. Abundant literature describes the spectrum of sub-arc mantle sources,
122 incorporating slab sedimentary components beneath Nicaragua, to volcanic seamounts
123 derived from Galapagos underneath Costa Rica and Panama (Carr et al., 2003; Gazel et al.,
124 2009; Hoernle et al., 2008; Patino et al., 2000; Ranero and von Huene, 2000;
125 Schwarzenbach et al., 2016).

126 Eight gas samples from fumaroles were collected from Poás and Momotombo
127 volcanoes during several field expeditions in the early to mid-2000's with gas chemistry
128 and isotope data published in Zimmer et al. (2004), Elkins et al. (2006), De Leeuw et al.,
129 (2007) and Fischer et al. (2015). Fumaroles had outlet temperatures ranging from 98°C to
130 747°C. Samples were collected in pre-evacuated Giggenbach bottles filled with 5N NaOH
131 solution (Giggenbach and Goguel, 1989). Gas splits were taken from the headspace of the
132 bottles with sealed glass tubes shortly after sample collection and stored until analyzed for
133 this work. Five gases from the Poás crater were collected between 2003 and 2006, from the
134 fumarolic sites "Official" and "Naranja", at temperatures between 98°C and 158°C. For
135 these, we report new N₂ isotopologue and ⁴⁰Ar/³⁶Ar data. ³He/⁴He of these samples are
136 7.0±0.2 R_A (Hilton et al., 2010) where R_A is air ³He/⁴He or 1.384 x 10⁻⁶. Gas chemistry is
137 available from previous work (Fischer et al., 2015). One fumarole sample was collected at
138 Santa Ana Volcano (Salvador), with a vent temperature of 400°C. It has a helium isotope
139 ratio of 7.5±0.1 R_A (De Leeuw et al., 2007). The He-Ne-Ar abundances are known (De
140 Leeuw et al., 2007). No ⁴⁰Ar/³⁶Ar is available but other gases from El Salvador all have

141 near-atmospheric $^{40}\text{Ar}/^{36}\text{Ar}$ ratios (Snyder et al., 2003). We additionally discuss two
142 fumarole gas samples collected at Momotombo in Nicaragua, at an outlet temperature of
143 $\sim 750^\circ\text{C}$. For these two samples, we report new $^{40}\text{Ar}/^{36}\text{Ar}$ isotope measurements. N_2
144 isotopologues, helium isotopes, He-Ne-Ar and major gas chemistry data for these samples
145 are available from previous work (Elkins et al., 2006; Yeung et al., 2017). Hot springs found
146 in the flanks of volcanic arcs are the most accessible samples, and hence are routinely used
147 to characterize volcanic endmembers (e.g. Snyder et al., 2003). As a means to compare
148 these to our fumaroles, we also report data from seven gases from bubbling springs in
149 Costa Rica and Panama, collected in 2018 as part of the *Biology Meets Subduction* initiative.
150 Sample collection sites are shown on [figure 1](#). Samples were collected in 15 cm^3 copper
151 tubes following standard procedures. Waters in the springs had temperatures between
152 29°C and 55°C . For these, we report major element gas compositions, N_2 isotopologues and
153 He-Ne-Ar systematic data.

154 **3. Methods**

155 Gas aliquots were split up to three ways and processed for (1) gas chemistry, (2) N_2 ,
156 and (3) noble gases systematics. Inorganic gas components (such as N_2 , He, Ar and O_2) and
157 methane were separated and quantified on a TCD gas chromatograph coupled with a
158 quadrupole mass spectrometer as in earlier work (Fischer et al., 2015). This allowed
159 determining the N_2/He and N_2/Ar ratios of each gas splits. Nitrogen isotopologues were
160 determined via high-resolution mass spectrometry at the University of California, Los
161 Angeles (Young et al., 2016). Noble gas analyses were conducted at the University of Oxford
162 (UK) and at the University of New Mexico using standard methods (Barry et al., 2016; Lee
163 et al., 2017). Details may be found in the [supplementary online file](#).

164

165 **4. Results**

166 We present an integrated dataset that includes concentrations of He, Ne, Ar, N₂, O₂,
167 and CH₄, elemental ratios of those gases, noble gas isotope compositions, and N₂
168 isotopologue ratios. Data for the fumaroles (n=8) are in **table 1** and data for the springs
169 (n=7) are in **table 2**.

170

171

172 **4.1. $\delta^{15}\text{N}$ and Δ_{30} relationships**

173 Newly determined Δ_{30} values vary between $19.3\pm 0.4\text{‰}$ and $3.5\pm 1.0\text{‰}$ (**1 σ**
174 **uncertainty, Fig. 2**). Two previously published data points from Momotombo extend the
175 range down to $1.5\pm 0.6\text{‰}$ and are plotted on Fig. 2 (Yeung et al. 2017). The highest Δ_{30} is
176 similar to the air value of $19.1\pm 0.3\text{‰}$ (2σ). The range in Δ_{30} values suggests samples
177 incorporate variable amounts of atmospheric nitrogen, contributing between ~ 8 and
178 $\sim 100\%$ of the total N₂. Fumaroles from Poás and Momotombo have the lowest Δ_{30} values,
179 indicating that these fumaroles have the lowest air-derived N₂ contributions. A range of
180 $\delta^{15}\text{N}$ values is observed, with values of between $-3.7\pm 0.3\text{‰}$ and $+4.2\pm 0.3\text{‰}$ (**Fig. 2**). For
181 Poás and Momotombo, $\delta^{15}\text{N}$ values are $+0.4\pm 0.3\text{‰}$ and $+5.4\pm 0.3\text{‰}$ respectively, where air
182 contributions are at their lowest values (minimum Δ_{30}). The $\delta^{15}\text{N}$ values as a whole (with
183 both low and high Δ_{30}) are within the range of $\delta^{15}\text{N}$ values of between -3.0 ± 0.6 and
184 $6.3\pm 0.3\text{‰}$ (n=73) reported previously for central American gases (Elkins et al., 2006;
185 Fischer et al., 2015, 2002; Snyder et al., 2003; Zimmer et al., 2004). The $\delta^{15}\text{N}$ values exhibit
186 a negative correlation with Δ_{30} values (**Fig. 2**).

187 4.2. Noble gas isotopes

188 Concentrations of He, Ne and Ar vary over 4 orders of magnitude and are correlated
189 (Table 1 and 2). We observe $^{40}\text{Ar}/^{36}\text{Ar}$ ratios between 297 ± 5 and 342 ± 5 for our samples
190 (Table 1 and 2), far from the upper mantle value of $\sim 25,000$ (Moreira et al. 1998) but close
191 to air at 298.5 (Lee et al., 2006). This is comparable to the known range of values for
192 Central American rocks and gases of between 292 ± 7 and 310 ± 5 (Fischer et al., 2005;
193 Kennedy et al., 1991; Snyder et al., 2003; Staudacher and Allègre, 1988). The $^{20}\text{Ne}/^{22}\text{Ne}$ and
194 $^{21}\text{Ne}/^{22}\text{Ne}$ ratios are known only for the hot springs, and data appear indistinguishable
195 from air (Table 2).

196 The $^3\text{He}/^4\text{He}$ ratios vary substantially, between 0.3 and $7.6\pm 0.1 R_A$. Unlike Ne and Ar,
197 the He budget is not significantly affected by atmospheric components and instead reflect
198 appreciable deep contributions. The $^3\text{He}/^4\text{He}$ ratios are broadly correlated with $^4\text{He}/^{20}\text{Ne}$
199 ratios (Fig. 3). Most of the data are explained by two-component mixing between air
200 ($^3\text{He}/^4\text{He} = 1 R_A$ by definition, $^4\text{He}/^{20}\text{Ne} = 0.3188$) and a magmatic endmember. The
201 magmatic component has a $^3\text{He}/^4\text{He}$ of ~ 7 (Fig. 3). The $^4\text{He}/^{20}\text{Ne}$ ratio of the magmatic
202 component must be at least as high as the highest value from our dataset, ~ 270 . Three
203 Costa Rican springs show a clear offset from the two-component mixing line, showing
204 much lower $^3\text{He}/^4\text{He}$ ratios at a given $^4\text{He}/^{20}\text{Ne}$ value. Similar features in other Central
205 American gases were interpreted to result from mixing with gases from crustal fluids (De
206 Leeuw et al., 2007).

207 4.3. Nitrogen, oxygen and methane concentrations

208 Nitrogen concentrations vary from 0.2 vol% to 93 vol% in the springs, and from 0.6
209 vol% to 1.9 vol% in the fumaroles (Table 1 and 2). Oxygen concentrations are variable,

210 resulting in O_2/N_2 ratios ranging over two orders of magnitude, between 3.8×10^{-4} to $1.1 \times$
211 10^{-1} (Supplementary Fig. 1). The O_2/N_2 ratios are not directly correlated with Δ_{30} values
212 (supplementary Fig. 1), suggesting that O_2/N_2 is not a reliable indicator of the presence of
213 nitrogen from air. Methane concentrations are below 0.1 vol % for most samples, with the
214 exception of two of the Costa Rica hot springs, where CH_4 concentrations are as high as ~ 80
215 vol %, suggesting contributions from shallow crustal gases (Snyder et al. 2003). N_2/CH_4
216 varies over 5 orders of magnitude, between $\sim 1.2 \times 10^{-1}$ to $\sim 2.1 \times 10^4$, but remains
217 uncorrelated with Δ_{30} values (Supplementary Fig. 1).

218 4.4. Nitrogen - noble gas ratios

219 We compute N_2/Ar , $N_2/^{36}Ar$, N_2/He and $N_2/^3He$ ratios, with a $\pm 20\%$ relative
220 uncertainty on individual samples. N_2/Ar ratios are between 21 and 120 for most samples,
221 with one sample from Momotombo at 507 (Fig. 4). For comparison, the air value is ~ 84 ,
222 air-saturated water (ASW) at STP is ~ 41 , and MORB gases have N_2/Ar ratios of 55 ± 5 (Javoy
223 and Pineau, 1991), although a higher estimate of $\sim 120 \pm 40$ (Marty and Dauphas, 2003) was
224 derived from MORB samples with unusually radiogenic $^{40}Ar/^{36}Ar$ ratios (data from Marty
225 et al., 1999). For samples where $^{40}Ar/^{36}Ar$ was measured, $N_2/^{36}Ar$ ratios vary between
226 1.2×10^4 and 4.2×10^4 . Assuming the $^{40}Ar/^{36}Ar$ is atmospheric as for other Central
227 American gas samples (Snyder et al., 2003), the $N_2/^{36}Ar$ range extends to between
228 6.5×10^3 and 1.5×10^5 (Fig. 4). This includes values below and above both air (2.5×10^4)
229 and air-saturated water at STP (1.3×10^4). The highest $N_2/^{36}Ar$ value remains well below
230 estimates of the convective mantle of $\sim 2 \times 10^6$ (Labidi et al., 2020; Marty and Humbert,
231 1997) even for samples where Δ_{30} is low.

232 The N_2/He ratios vary between 1.5×10^2 and 4.2×10^4 , below the value of air of
233 1.5×10^5 or air-saturated water $\sim 3.0 \times 10^5$ (Fig. 5). Similarly, $N_2/^3He$ ratios vary between
234 1.6×10^7 and 1.1×10^{11} (Fig. 5), mostly below the value of air and ASW of 1.0×10^{11} and
235 $\sim 2.0 \times 10^{11}$ respectively (Ballentine et al., 2002). The N_2/He (and $N_2/^3He$ ratios) are
236 correlated with Δ_{30} values and are described by two-component mixing hyperbolae
237 between air (or air-saturated waters) and high-temperature components with elevated
238 N_2/He (and $N_2/^3He$ ratios) relative to MORB gases (Fig. 5).

239 4.5. Noble gas ratios

240 The $^3He/^22Ne$ ratios range over 4 orders of magnitude, between 8.9×10^{-6} and
241 2.7×10^{-2} (Fig. 6). These values are between air, at 4.5×10^{-6} , and upper-mantle gases at
242 $\sim 5.5 \times 10^1$ (Moreira et al., 1998). The $^4He/^20Ne$ ratios are also ranging between air and the
243 upper-mantle value (Supplementary Figure 2). $^3He/^22Ne$ (and $^4He/^20Ne$) ratios are
244 correlated with Δ_{30} values (Fig. 6, Supp Fig. 2). At $\Delta_{30} = 0$ the high-temperature component
245 appears to have He/Ne ratios lower than MORB gases by about four orders of magnitude
246 (Fig. 6, Supp Fig. 2). The $^3He/^36Ar$ ratio ranges between 1.6×10^{-6} and 1.7×10^{-4} (Fig. 6).
247 This is higher than the air value of 2.5×10^{-7} , but considerably lower than the upper-
248 mantle value of $\sim 5.0 \times 10^{-1}$ (Moreira et al., 1998; Raquin et al., 2008). A similar
249 observation can be made of the $^4He/^40Ar$ ratio (Supp Fig. 2). The variations in $^3He/^36Ar$
250 (and $^4He/^40Ar$) ratios are correlated with Δ_{30} values and at $\Delta_{30} = 0$, the high-T component
251 shows $^3He/^36Ar$ ratios lower than MORB gases by about three orders of magnitude (Fig. 6,
252 Supp Fig. 2). Most $^{22}Ne/^36Ar$ ratios in fumaroles and springs range between 1.3×10^{-1} and
253 3.1×10^{-3} (with one outlier at $\sim 6.5 \times 10^{-1}$, the Poás gas with the Δ_{30} value closest to air).
254 The higher values are similar to the air and MORB values of 5.0×10^{-2} and 1.0×10^{-1} ,

255 respectively (Mukhopadhyay, 2012) and are observed for samples with air-like Δ_{30} values.
256 At $\Delta_{30} = 0$, much lower $^{22}\text{Ne}/^{36}\text{Ar}$ values are observed, lower than both MORB and air by
257 one to two orders of magnitude (Table 1 and 2).

258

259 **5. Discussion**

260 Our rationale is that correlations between Δ_{30} and various isotope and element ratios
261 can be used to identify and correct for air components and reveal pristine high-
262 temperature endmembers. Air is identified with a Δ_{30} of $19.1 \pm 0.3\text{‰}$, while any N_2
263 produced by a geologic process such as magmatic degassing has $\Delta_{30} \sim 0\text{‰}$ (Labidi et al.,
264 2020). Arguments against re-ordering and crustal contamination are given in the
265 supplementary discussion.

266

267 **5.1 Atmospheric N_2 may easily go unnoticed**

268 CAVA gas Δ_{30} values are variable, indicating commensurately variable contributions of
269 air to the N_2 budgets in hydrothermal discharges. Based on Δ_{30} data, air accounts for 40 to
270 100% of the N_2 in the springs. In fumaroles, air accounts for 8 to 90% of the N_2 .
271 Atmospheric N_2 is therefore ubiquitous. Systematics involving $\delta^{15}\text{N}$, $[\text{O}_2]$, O_2/N_2 , N_2/He and
272 N_2/Ar ratios may disentangle magmatic N_2 from air-derived N_2 in gas discharges (Sano et
273 al., 2001, Fischer et al. 2002, Elkins et al., 2006). The rationale for all of those approaches is
274 that air has known $\delta^{15}\text{N}$, O_2/N_2 , N_2/He and N_2/Ar ratios, that are different from magmatic
275 components. Our Δ_{30} data present a series of challenges to these previous approaches. For
276 example, samples with high $^4\text{He}/^{20}\text{Ne}$ ratios were suggested to illustrate a volatile budget
277 largely uncontaminated by air, especially when a number of other criteria are met, e.g.,

278 O_2/N_2 ratios $< 10^{-3}$, high outlet temperatures, or non-atmospheric N_2/Ar ratios (Elkins et
279 al., 2006). The Santa Ana volcano fumarole is vented at $400^\circ C$, a $^4He/^{20}Ne \sim 200$ times
280 higher than air and a O_2/N_2 ratio of $\sim 10^{-4}$ (Table 1, Fig. 3), which would suggest minimal air
281 contamination. However, the near-air Δ_{30} of $15.5 \pm 0.3\text{‰}$ requires that $\sim 80\%$ of N_2 is from
282 air in this sample, showing that high $^4He/^{20}Ne$, even in conjunction with high vent
283 temperature and low O_2/N_2 , is not necessarily sufficient evidence that N_2 is dominantly
284 magmatic (See supplementary discussion).

285

286

287 5.2 Atmospheric N_2 undergoes isotopic fractionation in hydrothermal systems

288 Nitrogen isotope ratios could be a direct tracer of atmospheric N_2 , since air and
289 magma-derived nitrogen are thought to have distinct $\delta^{15}N$ values (Fischer et al., 2002, Sano
290 et al., 2001). The Δ_{30} data confirm the veracity of this approach for most, but not all,
291 samples. Gases (except those from Poás) fall on a single two-component mixing trend
292 between air and a high-temperature component with near-zero Δ_{30} and $\delta^{15}N$ of $\sim 5\text{‰}$ (Fig.
293 2). For those, the air component appears unfractionated with respect to $\delta^{15}N$. When mixed
294 with high-temperature volatiles, $\delta^{15}N$ increases and Δ_{30} values decrease (Fig. 2).

295 Samples from Poás are different. They form a unique linear mixing trend where both
296 air-derived and high-temperature N_2 are distinct from elsewhere in the arc system, with
297 $\delta^{15}N$ endmember values of $-4.0 \pm 0.3\text{‰}$ and $+1.0 \pm 0.3\text{‰}$ for air and the high-T component,
298 respectively (Fig. 2). This represents a $\sim 4\text{‰}$ shift for both endmembers compared to
299 values observed elsewhere on the arc. Our observation creates ambiguities at Poás, since
300 there, and there only: (1) high-temperature $\delta^{15}N$ is only marginally higher than air; and (2)

301 air-derived N₂ has a δ¹⁵N very similar to the MORB value of -5±2‰ (Javoy and Pineau,
302 1991, Marty et al., 1999).

303 The data from Poás require that atmospheric N₂ experienced a ~4‰ mass-dependent
304 ¹⁵N/¹⁴N fractionation in the sub-surface. This may result from the degassing of once air-
305 saturated waters. The isotopic fractionation associated with N₂ dissolved in water was
306 experimentally documented to be +0.9 to -0.4 ‰ from 6 to 60 °C (Lee et al., 2015). The
307 dissolved-gas isotope fractionation was shown to cross over at about 40 °C, from a positive
308 to a negative sign (Lee et al., 2015). Above 40 °C, the isotopic difference between dissolved
309 and gaseous N₂ increases: isotopically light N₂ is increasingly partitioned in the dissolved
310 fraction as temperature increases. This behavior indicates that a kinetic isotope effect
311 attends N₂ dissolution/degassing in geothermal waters (Lee et al., 2015). Using the
312 experimental results of Lee et al., (2015), we calculate the consequences of N isotope
313 fractionation during open-system degassing using Rayleigh fractionation. At 60 °C, with a
314 gas/dissolved-gas ¹⁵N/¹⁴N fractionation factor of 1.0004, the lowest δ¹⁵N values of ~ -3.5
315 ‰ with air-like Δ₃₀ require that the N₂ sampled by the fumaroles is the residuum left over
316 after degassing of about 99.98 % of the dissolved nitrogen. Extrapolating the temperature
317 dependence of the fractionation factor to 100 °C, 97% degassing of N₂ is required to
318 account for a δ¹⁵N of ~ -3.5 ‰.

319 We envision the hydrothermal degassing to be the natural consequence of
320 hydrothermal systems experiencing continuous degassing in the absence of continuous
321 meteoric (air-saturated) water recharge. It is puzzling however that among the sites we
322 sampled, air nitrogen undergoes isotopic fractionation only at Poás. In order to explain this
323 observation, we suggest a restricted set of conditions is met in the Poás subsurface, but not

324 elsewhere. Gases from Momotombo and Santa Ana are vented at temperatures between
325 747 °C and 400 °C, respectively. No liquid water remains stable at those temperatures.
326 Thus, isotope partitioning between water and gas is not occurring, and N₂ remains
327 unfractionated. Spring gases are vented at temperatures between 29 °C and 59 °C (Table 2),
328 at temperatures where degassing is probably limited. In contrast, at Poás, the fumaroles are
329 vented at ~100-150 °C (Fischer et al., 2015). At these temperatures, liquid and gaseous
330 water are stable and water/gas partitioning can occur. These conditions are comparable to
331 those observed for hydrothermal gases from Iceland or Yellowstone, where negative $\delta^{15}\text{N}$
332 values were previously observed in conjunction with air like Δ_{30} values (Labidi et al., 2020).
333 Our conclusion is also consistent with the observation of sporadically negative $\delta^{15}\text{N}$ (with
334 no available Δ_{30} data) in Poás fumaroles sampled in 2001. Values as low as $\sim -3.0\text{‰}$ were
335 observed in fumarole vented at temperature between 76 and 108 °C (Fischer et al., 2002).
336 In other fumaroles (89-101 °C) sampled between 1998 and 2001, while unfractionated air-
337 like $\delta^{15}\text{N}$ and N₂/Ar values were reported (Vaselli et al., 2003). More work is warranted to
338 follow the potential Δ_{30} - $\delta^{15}\text{N}$ evolution of a given fumarole through time, but in the interim,
339 we suggest caution in interpreting $\delta^{15}\text{N}$ data at Poás in the absence of Δ_{30} .

340

341 **5.3. Is high-temperature nitrogen also fractionated?**

342 Whether high-temperature components with $\Delta_{30} \sim 0\text{‰}$ also experience $\delta^{15}\text{N}$ isotope
343 fractionation in hydrothermal systems is an open question. At Momotombo, fumaroles have
344 a high-temperature endmember with $\delta^{15}\text{N} \sim +5\text{‰}$ (Fig. 2.). There, vent temperatures are >
345 700 °C. This precludes liquid water to exist even at depths, ruling out the possibility of any
346 water/gas isotope exchange. This is consistent with a previous observation of

347 unfractionated $\delta^{15}\text{N}$ for fumaroles when they are vented at $> 300\text{ }^\circ\text{C}$ (Fischer et al., 2005).
348 At Poás however, the interpretation is not as straightforward, where the high-temperature
349 endmember has a $\delta^{15}\text{N} \sim +1\text{‰}$ (Fig. 2), which is lower than at Momotombo by $\sim 4\text{‰}$,
350 implying that a fractionation similar to that for the air component could have occurred. It
351 is conceivable that high-T volatiles have been delivered to the water table *prior to*
352 hydrothermal degassing, where they would experience $^{15}\text{N}/^{14}\text{N}$ fractionation together with
353 the air-derived gases. In this interpretation, the high-T $\delta^{15}\text{N}$ value of $\sim +1\text{‰}$ obtained by
354 extrapolation to $\Delta_{30} = 0$ would not record the actual magmatic $\delta^{15}\text{N}$ value at Poás, and the
355 Poás trend would be parallel to the main array as the result of a fractionation equally
356 affecting both the atmospheric and high-T volatiles. However, with our dataset alone, we
357 cannot exclude that high-T volatiles had been delivered to the fumaroles *after*
358 hydrothermal degassing. If so, the Poás high-T endmember could be truly unique in $\delta^{15}\text{N}$,
359 and the Poás trend being parallel to the main array (Fig. 2) would be fortuitous. This latter
360 scenario relies on a coincidence, and thus appears unlikely, although it cannot be fully ruled
361 out.

362

363 **5.4. N_2/Ar ratios place independent constraints on hydrothermal degassing**

364 The solubilities of argon and nitrogen are distinct by about a factor of 2 in geothermal
365 waters at temperatures between 20 and 100 $^\circ\text{C}$ (Ballentine et al, 2002). Thus, water/gas
366 processes may be tracked with N_2/Ar ratios, independently of nitrogen isotopes. Low
367 N_2/Ar ratios for air-like Δ_{30} values are observed at Poás, while most other samples have
368 near-air values for N_2/Ar at air-like Δ_{30} (Fig. 4), confirming that at Poás liquid-gas

369 partitioning occurred in the sub-surface. We can again use a Rayleigh fractionation
370 calculation to infer the amount of degassing implied by the N₂/Ar ratio data, where

371
$$N_2/Ar = (N_2/Ar)_0 f^{\alpha-1} \quad (1)$$

372 and

373
$$\alpha = (K_{N_2}/K_{Ar}), \quad (2)$$

374 where f is the fraction of remaining Ar in the water, $(N_2/Ar)_0$ the known starting
375 composition of ASW, and α is the fractionation coefficient given for a gas/liquid system
376 given by Equation (2), and K_i is the Henry's-law constant for species i , as compiled in
377 Ballentine et al., (2002). Taking $(N_2/Ar)_0$ to be 41, we find that the lowest N₂/Ar value of ~
378 10 implied by our data occurs for about 94% degassing of N₂ (75% degassing of Ar) prior
379 to sampling (Fig. 4). To first order, this degree of degassing is consistent with estimates
380 made on the basis of ¹⁵N/¹⁴N values (section 5.2).

381 There is a caveat to this interpretation. Data for $\delta^{15}N$ and N₂/Ar appear consistent
382 with fractionation within hydrothermal systems, but no direct correlation is observed
383 between $\delta^{15}N$ and N₂/Ar (Table 1). This is perhaps because degassing may yield variable
384 ¹⁵N/¹⁴N and N₂/Ar fractionations depending on the exact temperature and pressure
385 conditions (Lee et al., 2015; Warr et al., 2015). Under conditions making the gas behavior
386 non-ideal, degassing may change the N₂-Ar solubility relationship, as suggested for heavier
387 noble gases (Labidi et al., 2020, Warr et al., 2015). Additionally, small contributions of high-
388 temperature volatiles are likely to cause shifts in $\delta^{15}N$ with no obvious increases in N₂/Ar
389 ratios (Fig. 4). This is because high-temperature endmembers with $\Delta_{30} = 0\text{‰}$ appear to
390 have N₂/Ar and N₂/³⁶Ar ratios of ~ 100 and ~ 10⁴, respectively (Fig. 4). These values are

391 essentially similar to air, consistent with pioneer work on the CAVA (Hilton et al., 2002;
392 Snyder et al., 2003), but remain lower than volcanic endmembers at other arcs (Taran,
393 2009; Zelenski and Taran, 2011). We note that one of the Momotombo fumaroles has a high
394 N_2/Ar of ~ 500 , higher than other high-temperature gases by a factor of 5. The significance
395 of variable N_2/Ar ratios in Central American high-temperature endmembers must be
396 systematically investigated in future work, with Δ_{30} data.

397

398 **5.5. $\delta^{15}N$ - N_2/He relationships constrained by Δ_{30} data**

399 In contrast to argon, the solubility of helium in geothermal waters is nearly
400 indistinguishable from that of nitrogen in the relevant temperature range (Ballentine et al.,
401 2002). Data can be accounted for by mixing between air and an endmember with $N_2/^3He$
402 ratios $\sim 10^8$ (Fig. 5). This is higher than MORB gases that are characterized by $N_2/^3He$
403 ratios of about 10^6 (Javoy and Pineau, 1991, Marty and Humbert, 1999). The Poás
404 fumaroles involve a mixing scenario that is similar to the one for Momotombo, involving
405 high-T endmembers with a $N_2/^3He$ of $\sim 10^8$ (Fig. 5). This observation argues against a
406 significant contribution of MORB derived volatiles to Poás volcanic gas discharges. Overall
407 light $\delta^{15}N$ values from Poás were previously suggested to reflect a contribution from
408 MORB-derived volatiles, contrary to the majority of other CAVA gas discharges that showed
409 predominantly slab-derived N (Fischer et al., 2002, Elkins et al., 2006). Our new Δ_{30} data
410 suggest a revision to the interpretation of ^{15}N depletions and show that they rather reflect
411 contributions of fractionated air (Fig. 2) mixed with a predominantly non-MORB magmatic
412 component with elevated N_2/He ratios (Fig. 5).

413

414 5.6. Magmatic endmembers throughout the arc are enriched in N₂

415 In an attempt to characterize subduction volatiles, we constrain the high-temperature
416 endmembers for nitrogen isotopes and N₂/Ar, N₂/He, He/Ne and He/Ar ratios.
417 Endmember compositions are calculated assuming two-component mixing with air
418 constrained by Δ_{30} values, as described above. We focus on fumarole data to constrain
419 endmember compositions, since they show the lowest Δ_{30} and no evidence of crustal
420 contamination (see supplementary discussion).

421 The derived N₂/He ratios are higher than MORB by two orders of magnitude. In
422 contrast, He/Ne, He/Ar and N₂/³⁶Ar are all lower than MORB by two to three orders of
423 magnitude (Fig. 4-6). The simplest explanation is that slab-derived N₂, Ne and Ar were
424 added to a depleted mantle source with an unmodified helium signature (Fig. 7). A
425 straightforward quantification of slab-derived N₂, Ar and Ne to the mantle wedge is
426 possible using N₂/³He, ³He/²²Ne and ³He/³⁶Ar ratios. This approach is viable if ³He
427 subduction is negligible (Staudacher and Allegre, 1988), notwithstanding that slab
428 components are required to contribute minute ⁴He ingrowth from subducted uranium
429 (Hilton et al., 2002).

430 The high-T, arc magma endmembers at Poás and Momotombo have N₂/³He ratios two
431 orders of magnitude higher than MORB, requiring nitrogen addition to mantle sources in
432 these arc systems. Sedimentary nitrogen may be a straightforward contributor to the
433 Momotombo source, explaining the high $\delta^{15}\text{N}$ of + 5‰ there (Fig. 7). Sediments on the
434 modern oceanic crust directly offshore of Central America are likely candidates, since they
435 have an average $\delta^{15}\text{N}$ of ~5‰ (Li and Bebout, 2005). Poás volcano is more complicated,
436 because the lower $\delta^{15}\text{N}$ (Fig. 2) may not be a genuine representation of the Poás mantle

437 source. We note that because $N_2/{}^3\text{He}$ are indistinguishable between Poás and Momotombo,
438 they must have received a comparable amount of slab-derived N.

439 Sub-arc magmatic endmembers have lower ${}^3\text{He}/{}^{22}\text{Ne}$ and ${}^3\text{He}/{}^{36}\text{Ar}$ ratios by 2 to 3
440 orders of magnitude compared to those of MORBs. Like nitrogen, this likely requires
441 substantial addition of slab-derived neon and argon to a mantle source. Samples with near-
442 zero Δ_{30} have ${}^{22}\text{Ne}/{}^{36}\text{Ar}$ lower than both MORB and air by one to two orders of magnitude
443 (Table 1), with values trending toward $\sim 0.7 \times 10^{-2}$. This is similar to the median ratio of
444 an entire section of altered oceanic crust and sediments of $\sim 1 \times 10^{-2}$ (Chavrit et al., 2016).
445 The similarity in ${}^{22}\text{Ne}/{}^{36}\text{Ar}$ between the magmatic endmembers at CAVA and the slab is
446 consistent with a mantle wedge being overwhelmed by the addition of slab-derived neon
447 and argon. Samples with near-zero Δ_{30} also have atmospheric ${}^{40}\text{Ar}/{}^{36}\text{Ar}$ values (Table 1),
448 indicating that Ar from the mantle wedge has retained the noble gas isotopic signature of
449 its subducted atmospheric source. This is likely explained by the contribution of surface-
450 derived argon with atmospheric ${}^{40}\text{Ar}/{}^{36}\text{Ar}$ ratios to the mantle wedge. This sheds new light
451 on atmospheric ${}^{40}\text{Ar}/{}^{36}\text{Ar}$ observed systematically in all known Central American
452 fumaroles (Snyder et al. 2003) and essentially all gas discharges sampled to date from
453 subduction zones (Hilton et al., 2002, Sano and Fischer, 2013): A likely origin for the
454 atmospheric Ar in high-T endmembers is devolatilizing subducted protoliths that are
455 otherwise known to have atmospheric Ar isotopic signatures (Chavrit et al., 2016; Holland
456 and Ballentine, 2006; Staudacher and Allègre, 1988). Our high-T data shows that not all of
457 the subducted air-derived Ar is transferred into the deeper mantle and that some of it is
458 released via arc volcanism. Our data also dispels the notion that atmospheric Ar-isotope

459 signatures of arc-gases are exclusively the result of shallow atmospheric contamination in
460 the hydrothermal system.

461

462 **5.7 Revisiting volatile fluxes in the central American subduction zone.**

463 The perspective that volatiles from the mantle wedge incorporate recycled argon is
464 problematic, as it limits the use of nitrogen excesses, N_2^* , calculated on the basis of N_2/Ar
465 ratios (Fischer et al. 1998,2002, Hilton et al., 2002). We show here that magmatic volatiles
466 deliver measurable amounts of argon (with atmospheric $^{40}Ar/^{36}Ar$) to the fumaroles.
467 Consequently, assumptions on N_2^* may naturally underestimates the outgassing flux of N_2 .
468 Estimates for the fluxes of N_2 , Ar, and Ne can be obtained from 3He degassing fluxes. Using a
469 combination of S/CO_2 , He/CO_2 and $^3He/^4He$ ratios, and an SO_2 flux of 21.3×10^9 mol/yr,
470 Hilton et al. (2002) derived a 3He flux of 5.4 mol/yr for the entire CAVA. Using the CAVA
471 CO_2 flux from Fischer et al., (2019) of 94×10^9 mol/yr, and a $CO_2/^3He$ ratio of 2×10^{10}
472 (Kagoshima et al., 2015), we obtain a 3He flux 4.7 mol/yr. Here, we take a 3He flux of 5.0
473 mol/yr for the sake of illustration. We combine our new elemental ratios estimates for the
474 CAVA source (Fig. 4-6) with 3He fluxes to derive new estimates for N_2 , ^{36}Ar , and ^{22}Ne
475 outgassing fluxes in the central American arc.

476 We derive $N_2/^3He$ ratios between 8×10^7 and 2×10^8 for magmatic volatiles in Central
477 America (Fig. 5), from samples with $\Delta_{30} < 5\text{‰}$. This results in a N_2 flux between 4.0×10^8
478 and 1.0×10^9 mol N_2/y (or 1.1×10^{10} and 2.8×10^{10} g N/y). This range for the nitrogen mass
479 flux is higher than previous estimates of 8.2×10^9 g N/y (Fischer et al., 2002, Hilton et al.,
480 2002). Our derived range of nitrogen fluxes overlaps the estimated flux of subducting
481 nitrogen of 1.6×10^{10} g N/y (1.1×10^9 mol N/y , or 5.7×10^8 mol N_2/yr), given with no

482 uncertainty in Busigny et al. (2019) and Li and Bebout (2005). This suggests that in the
483 Central American subduction zone, the N₂ cycle is not required to be out of equilibrium.
484 Instead, the revisited fluxes being identical within uncertainty, they allow N₂ to be
485 quantitatively recycled through the mantle wedge and returned to the surface by degassing
486 rather than being delivered to the deep mantle. An additional source of outgassing
487 underestimation, here, is that we ignore forearc devolatilization for N₂, known to occur in
488 the CAVA (Inguaggiato et al., 2004). Future work will be necessary to constrain this fraction
489 of the N₂ flux that will inevitably increase the outgassing flux further. In any case, our newly
490 defined N₂ outgassing fluxes are high, and in the range of subducting fluxes. Because this
491 subduction zone is relatively “warm” and therefore more similar to subduction zones in the
492 past over geological timescales (Keller and Schoene, 2018; Martin and Moyen, 2002), the
493 finding that nitrogen is recycled by subduction and arc magmatism in the Central American
494 system suggests that nitrogen subduction could have been inefficient through geological
495 time. This conclusion is also in agreement with recent experimental work suggesting warm
496 subduction zones limit nitrogen recycling in the deep mantle (Jackson et al., 2021).

497 We estimate the ³He/³⁶Ar of magmatic inputs to be $\sim 10^{-4}$ (Fig. 6). A ³He/³⁶Ar ratio of
498 $\sim 10^{-4}$ leads to a degassing ³⁶Ar flux of $\sim 5.0 \times 10^4$ mol/y (1.8×10^6 g ³⁶Ar/y) in Central
499 America. Using 1.4×10^{16} g of subducted crust, depths of ~ 6 km of oceanic crust and ~ 500
500 m of sediments, and the noble gases abundances in the oceanic crust (Chavrit et al., 2016),
501 we derive a ³⁶Ar subduction flux of 1.1×10^8 cm³ STP/y, or 4.5×10^4 mol ³⁶Ar/y. Because of
502 the large uncertainties in ³⁶Ar concentrations in rocks (Chavrit et al., 2016), this subduction
503 flux estimate is probably associated with a $\sim 50\%$ uncertainty, and is presented here for
504 illustration only. We note however that subduction and outgassing ³⁶Ar flux compare

505 favorably. Like nitrogen, our flux analysis seems to allow quantitative release of slab-
506 derived ^{36}Ar to the mantle wedge, which would not require substantial ^{36}Ar recycling into
507 the deep mantle in this subduction zone. The same conclusion holds for neon. Using a
508 $^3\text{He}/^{22}\text{Ne}$ of $\sim 2 \times 10^{-2}$ (Fig. 6), we obtain a ^{22}Ne degassing flux of $\sim 2.5 \times 10^2$ mol/y (5.5×10^3
509 g $^{22}\text{Ne}/\text{y}$). The $^{22}\text{Ne}/^{36}\text{Ar}$ of subducting components is largely variable, around a mode of
510 $\sim 10^{-2}$ (Chavrit et al., 2016). This yields a ^{22}Ne subduction flux of 1.1×10^6 cm³ STP/y, or 4.5
511 $\times 10^2$ mol $^{22}\text{Ne}/\text{y}$. Again, although large uncertainties must be taken into consideration, the
512 neon subduction and degassing fluxes appear equivalent, arguing in favor of quantitative
513 ^{22}Ne recycling in the central American subduction zone back to the surface.

514 The simplest interpretation of the fluxes derived here is that the Central American
515 subduction zone acts as a subduction barrier for N, Ar, and Ne: volcanic fluxes for N₂, Ar,
516 and Ne, determined with the $^{15}\text{N}/^{14}\text{N}$ approach, *no longer require* subduction of these
517 elements past the sub-arc melting region in the central American subduction zone.

518

519

520 6. Conclusion

521 Gas discharges in Central America are volatile mixtures involving contributions from
522 at least three endmembers: air (\pm fractionated air), crust, and mantle-derived components.
523 Using Δ_{30} as a tracer of nitrogen from air in fumaroles and springs, we show that O₂/N₂
524 ratios are unreliable tracers of air in these systems. We also show that $\delta^{15}\text{N}$ and N₂/Ar
525 ratios experienced fractionation during water degassing at depth, rendering these
526 unreliable as signatures of air where liquid water is thermodynamically stable. This is
527 problematic since the degassing fractionation may lead to $\delta^{15}\text{N}$ values that insidiously

528 mimic MORB gases. This does not seem to affect magmatic components, but more work is
529 needed on Poás – where interaction with the hydrothermal system may be significant,
530 before a firm conclusion can be reached. A preliminary conclusion is that without Δ_{30} data,
531 the $\delta^{15}\text{N-N}_2\text{-Ar}$ systematics may be deceptive, and can lead to confusion with regard to the
532 origin of N_2 in mixed gases.

533 We derive estimates of N_2/He , He/Ar and He/Ne ratios that reliably exclude
534 atmospheric components. N_2 , Ar and Ne enrichments by two or three orders of magnitude
535 compared to a MORB source are observed. They are attributed to mantle wedge sources
536 incorporating slab-derived gases. Using known ^3He degassing fluxes, we calculated N_2 , Ne
537 and Ar degassing fluxes for the Central American arc that could balance subduction fluxes,
538 within uncertainties, no longer requiring the Central American arc to have heavily
539 imbalanced volatile cycles.

540

541

542

543 **Acknowledgement**

544 This study was supported by the Deep Carbon Observatory through Sloan Foundation
545 grant numbers G-2018-11346 to EDY. This work was also supported by grant G-2016-7206 from
546 the Alfred P. Sloan Foundation and the Deep Carbon Observatory to PHB. Karen Lloyd and
547 Donato Giovannelli are thanked for co-organizing the Subduction meets Biology initiative.
548 Further, we acknowledge the National Science Foundation (NSF) award MGG-2015789 to PHB.
549 We thank Yuri Taran and an anonymous reviewer for constructive and helpful comments.
550 Rosemary Hickey-Vargas is thanked for editorial handling.

551

552 **References**

- 553 Barry, P.H., Lawson, M., Meurer, W.P., Warr, O., Mabry, J.C., Byrne, D.J., Ballentine, C.J., 2016. Noble gases solubility models
554 of hydrocarbon charge mechanism in the Sleipner Vest gas field. *Geochim. Cosmochim. Acta* 194, 291–309.
- 555 Bebout, G.E., Agard, P., Kobayashi, K., Moriguti, T., Nakamura, E., 2013. Devolatilization history and trace element mobility
556 in deeply subducted sedimentary rocks: Evidence from Western Alps HP/UHP suites. *Chem. Geol.* 342, 1–20.
- 557 Bekaert, D.V., Turner, S.J., Broadley, M.W., Barnes, J.D., Halldórsson, S.A., Labidi, J., Wade, J., Walowski, K.J., Barry, P.H.,
558 2020. Subduction-Driven Volatile Recycling: A Global Mass Balance. *Annu. Rev. Earth Planet. Sci.* 49.
- 559 Busigny, V., Cartigny, P., Laverne, C., Teagle, D., Bonifacie, M., Agrinier, P., 2019. A re-assessment of the nitrogen
560 geochemical behavior in upper oceanic crust from Hole 504B: Implications for subduction budget in Central
561 America. *Earth Planet. Sci. Lett.* 525, 115735.
- 562 Busigny, V., Cartigny, P., Philippot, P., Ader, M., Javoy, M., 2003. Massive recycling of nitrogen and other fluid-mobile
563 elements (K, Rb, Cs, H) in a cold slab environment: evidence from HP to UHP oceanic metasediments of the Schistes
564 Lustrés nappe (western Alps, Europe). *Earth Planet. Sci. Lett.* 215, 27–42. [https://doi.org/10.1016/s0012-](https://doi.org/10.1016/s0012-821x(03)00453-9)
565 [821x\(03\)00453-9](https://doi.org/10.1016/s0012-821x(03)00453-9)
- 566 Carr, M.J., Feigenson, M.D., Patino, L.C., Walker, J.A., 2003. Volcanism and geochemistry in Central America: Progress and
567 problems. *Geophys. Monogr. Geophys. Union* 138, 153–174.
- 568 Chavrit, D., Burgess, R., Sumino, H., Teagle, D.A.H., Droop, G., Shimizu, A., Ballentine, C.J., 2016. The contribution of
569 hydrothermally altered ocean crust to the mantle halogen and noble gas cycles. *Geochim. Cosmochim. Acta* 183,
570 106–124.
- 571 De Leeuw, G.A.M., Hilton, D.R., Fischer, T.P., Walker, J.A., 2007. The He–CO₂ isotope and relative abundance characteristics
572 of geothermal fluids in el salvador and honduras: New constraints on volatile mass balance of the central american
573 volcanic arc. *Earth Planet. Sci. Lett.* 258, 132–146.
- 574 Elkins, L.J., Fischer, T.P., Hilton, D.R., Sharp, Z.D., McKnight, S., Walker, J., 2006. Tracing nitrogen in volcanic and
575 geothermal volatiles from the Nicaraguan volcanic front. *Geochim. Cosmochim. Acta* 70, 5215–5235.
- 576 Fischer, T.P., Hilton, D.R., Zimmer, M.M., Shaw, A.M., Sharp, Z.D., Walker, J.A., 2002. Subduction and recycling of nitrogen
577 along the Central American margin. *Science (80-.)*. 297, 1154–1157.
- 578 Fischer, T.P., Ramírez, C., Mora-Amador, R.A., Hilton, D.R., Barnes, J.D., Sharp, Z.D., Le Brun, M., de Moor, J.M., Barry, P.H.,
579 Füre, E., Shaw, A.M., 2015. Temporal variations in fumarole gas chemistry at Poás volcano, Costa Rica. *J. Volcanol.*
580 *Geotherm. Res.* 294, 56–70. <https://doi.org/10.1016/j.jvolgeores.2015.02.002>

581 Fischer, T.P., Takahata, N., Sano, Y., Sumino, H., Hilton, D.R., 2005. Nitrogen isotopes of the mantle: Insights from mineral
582 separates. *Geophys. Res. Lett.* 32.

583 Gazel, E., Carr, M.J., Hoernle, K., Feigenson, M.D., Szymanski, D., Hauff, F., Van Den Bogaard, P., 2009. Galapagos-OIB
584 signature in southern Central America: Mantle refertilization by arc-hot spot interaction. *Geochemistry, Geophys.*
585 *Geosystems* 10.

586 Hilton, D.R., Fischer, T.P., Marty, B., 2002. Noble gases and volatile recycling at subduction zones. *Rev. Mineral.*
587 *geochemistry* 47, 319–370.

588 Hilton, D.R., Ramirez, C.J., Mora-Amador, R., Fischer, T.P., Füre, E., Barry, P.H., Shaw, A.M., 2010. Monitoring of temporal and
589 spatial variations in fumarole helium and carbon dioxide characteristics at Poás and Turrialba volcanoes, Costa Rica
590 (2001-2009). *Geochem. J.* 44, 431–440.

591 Hoernle, K., Abt, D.L., Fischer, K.M., Nichols, H., Hauff, F., Abers, G.A., Van Den Bogaard, P., Heydolph, K., Alvarado, G., Protti,
592 M., 2008. Arc-parallel flow in the mantle wedge beneath Costa Rica and Nicaragua. *Nature* 451, 1094–1097.

593 Holland, G., Ballentine, C.J., 2006. Seawater subduction controls the heavy noble gas composition of the mantle. *Nature*
594 441, 186–191. <https://doi.org/10.1038/nature04761>

595 Inguaggiato, S., Taran, Y., Grassa, F., Capasso, G., Favara, R., Varley, N., Faber, E., 2004. Nitrogen isotopes in thermal fluids
596 of a forearc region (Jalisco Block, Mexico): Evidence for heavy nitrogen from continental crust. *Geochemistry,*
597 *Geophys. Geosystems* 5.

598 Jackson, C.R.M., Cottrell, E., Andrews, B., 2021. Warm and oxidizing slabs limit ingassing efficiency of nitrogen to the
599 mantle. *Earth Planet. Sci. Lett.* 553, 116615.

600 Javoy, M., Pineau, F., 1991. The volatiles record of a “popping” rock from the Mid-Atlantic Ridge at 14°N: chemical and
601 isotopic composition of gas trapped in the vesicles. *Earth Planet. Sci. Lett.* 107, 598–611.

602 Keller, B., Schoene, B., 2018. Plate tectonics and continental basaltic geochemistry throughout Earth history. *Earth Planet.*
603 *Sci. Lett.* 481, 290–304.

604 Kennedy, B.M., Hiyagon, H., Reynolds, J.H., 1991. Noble gases from Honduras geothermal sites. *J. Volcanol. Geotherm. Res.*
605 45, 29–39.

606 Labidi, J., Barry, P.H., Bekaert, D. V., Broadley, M.W., Marty, B., Giunta, T., Warr, O., Lollar, B.S., Fischer, T.P., Avice, G., 2020.
607 Hydrothermal ^{15}N abundances constrain the origins of mantle nitrogen. *Nature* 580, 367–371.

608 Lee, H., Fischer, T.P., Muirhead, J.D., Ebinger, C.J., Kattenhorn, S.A., Sharp, Z.D., Kianji, G., Takahata, N., Sano, Y., 2017.
609 Incipient rifting accompanied by the release of subcontinental lithospheric mantle volatiles in the Magadi and
610 Natron basin, East Africa. *J. Volcanol. Geotherm. Res.* 346, 118–133.

611 Lee, H., Sharp, Z.D., Fischer, T.P., 2015. Kinetic nitrogen isotope fractionation between air and dissolved N_2 in water:

612 Implications for hydrothermal systems. *Geochem. J.* 49, 571–573.

613 Lee, J.-Y., Marti, K., Severinghaus, J.P., Kawamura, K., Yoo, H.-S., Lee, J.B., Kim, J.S., 2006. A redetermination of the isotopic
614 abundances of atmospheric Ar. *Geochim. Cosmochim. Acta* 70, 4507–4512.

615 Li, L., Bebout, G.E., 2005. Carbon and nitrogen geochemistry of sediments in the Central American convergent margin:
616 Insights regarding subduction input fluxes, diagenesis, and paleoproductivity. *J. Geophys. Res. Solid Earth* 110.

617 Libourel, G., Marty, B., Humbert, F., 2003. Nitrogen solubility in basaltic melt. Part I. Effect of oxygen fugacity. *Geochim.*
618 *Cosmochim. Acta* 67, 4123–4135. [https://doi.org/10.1016/s0016-7037\(03\)00259-x](https://doi.org/10.1016/s0016-7037(03)00259-x)

619 Martin, H., Moyen, J.-F., 2002. Secular changes in tonalite-trondhjemite-granodiorite composition as markers of the
620 progressive cooling of Earth. *Geology* 30, 319–322.

621 Marty, B., Humbert, F., 1997. Nitrogen and argon isotopes in oceanic basalts. *Earth Planet. Sci. Lett.* 152, 101–112.

622 Mikhail, S., Sverjensky, D.A., 2014. Nitrogen speciation in upper mantle fluids and the origin of Earth's nitrogen-rich
623 atmosphere. *Nat. Geosci.* 7, 816–819. <https://doi.org/10.1038/ngeo2271>
624 <http://www.nature.com/ngeo/journal/v7/n11/abs/ngeo2271.html#supplementary-information>

625 Moreira, M., Kunz, J., Allegre, C., 1998. Rare gas systematics in popping rock: isotopic and elemental compositions in the
626 upper mantle. *Science* (80-.). 279, 1178–1181.

627 Mukhopadhyay, S., 2012. Early differentiation and volatile accretion recorded in deep-mantle neon and xenon. *Nature*
628 486, 101–104. <https://doi.org/10.1038/nature11141>

629 Patino, L.C., Carr, M.J., Feigenson, M.D., 2000. Local and regional variations in Central American arc lavas controlled by
630 variations in subducted sediment input. *Contrib. to Mineral. Petrol.* 138, 265–283.

631 Peacock, S.M., van Keken, P.E., Holloway, S.D., Hacker, B.R., Abers, G.A., Ferguson, R.L., 2005. Thermal structure of the Costa
632 Rica–Nicaragua subduction zone. *Phys. Earth Planet. Inter.* 149, 187–200.

633 Plank, T., Kelley, K.A., Zimmer, M.M., Hauri, E.H., Wallace, P.J., 2013. Why do mafic arc magmas contain ~ 4 wt% water on
634 average? *Earth Planet. Sci. Lett.* 364, 168–179.

635 Ranero, C.R., von Huene, R., 2000. Subduction erosion along the Middle America convergent margin. *Nature* 404, 748–752.

636 Raquin, A., Moreira, M.A., Guillon, F., 2008. He, Ne and Ar systematics in single vesicles: mantle isotopic ratios and origin of
637 the air component in basaltic glasses. *Earth Planet. Sci. Lett.* 274, 142–150.

638 Schwarzenbach, E.M., Gill, B.C., Gazel, E., Madrigal, P., 2016. Sulfur and carbon geochemistry of the Santa Elena peridotites:
639 Comparing oceanic and continental processes during peridotite alteration. *Lithos* 252–253, 92–108.
640 <https://doi.org/http://dx.doi.org/10.1016/j.lithos.2016.02.017>

641 Snyder, G., Poreda, R., Fehn, U., Hunt, A., 2003. Sources of nitrogen and methane in Central American geothermal settings:
642 Noble gas and ¹²⁹I evidence for crustal and magmatic volatile components. *Geochemistry, Geophys. Geosystems* 4,

643 1–28.

644 Staudacher, T., Allègre, C.J., 1988. Recycling of oceanic crust and sediments: the noble gas subduction barrier. *Earth*

645 *Planet. Sci. Lett.* 89, 173–183.

646 Taran, Y.A., 2009. Geochemistry of volcanic and hydrothermal fluids and volatile budget of the Kamchatka–Kuril

647 subduction zone. *Geochim. Cosmochim. Acta* 73, 1067–1094.

648 Vaselli, O., Tassi, F., Minissale, A., Montegrossi, G., Duarte, E., Fernandez, E., Bergamaschi, F., 2003. Fumarole migration and

649 fluid geochemistry at Poás volcano (Costa Rica) from 1998 to 2001. *Geol. Soc. London, Spec. Publ.* 213, 247–262.

650 Warr, O., Rochelle, C.A., Masters, A., Ballentine, C.J., 2015. Determining noble gas partitioning within a CO₂–H₂O system at

651 elevated temperatures and pressures. *Geochim. Cosmochim. Acta* 159, 112–125.

652 Yeung, L.Y., Li, S., Kohl, I.E., Haslun, J.A., Ostrom, N.E., Hu, H., Fischer, T.P., Schauble, E.A., Young, E.D., 2017. Extreme

653 enrichment in atmospheric ¹⁵N/¹⁵N. *Sci. Adv.* 3, eaao6741.

654 Young, E.D., Rumble III, D., Freedman, P., Mills, M., 2016. A large-radius high-mass-resolution multiple-collector isotope

655 ratio mass spectrometer for analysis of rare isotopologues of O₂, N₂, CH₄ and other gases. *Int. J. Mass Spectrom.*

656 401, 1–10.

657 Zelenski, M., Taran, Y., 2011. Geochemistry of volcanic and hydrothermal gases of Mutnovsky volcano, Kamchatka:

658 evidence for mantle, slab and atmosphere contributions to fluids of a typical arc volcano. *Bull. Volcanol.* 73, 373–

659 394.

660 Zimmer, M.M., Fischer, T.P., Hilton, D.R., Alvarado, G.E., Sharp, Z.D., Walker, J.A., 2004. Nitrogen systematics and gas fluxes

661 of subduction zones: insights from Costa Rica arc volatiles. *Geochemistry, Geophys. Geosystems* 5.

662

663

664 **Captions**

		PO 06-1-3	PO 03-2	Pnar 06-1	PO 06-1-1	PO 06-1-2	ES02 10	Nic-3	Nic-2
		Poas 11/5/06	Poas 3/31/03	Poas 2/24/06	Poas 2/24/06	Poas 2/24/06	Santa Ana	Momotombo 1/5/02	Momotomb 1/5/02
dates of collection									
latitude		10.12	10.12	10.12	10.12	10.12	13.5111	12.2519	12.2519
longitude		-84.1359	-84.1359	-84.1359	-84.1359	-84.1359	-89.3748	-86.3224	-86.3224
temperature (C°)		113	98	153	113	113	400	747	747
quantity of processed N ₂	10 ⁶ mol	2.1	2.2	8.8	8.0	5.8	22.4		
N ₂ vol fraction (ucla)	x10 ²	9.21E-01	8.47E-01	3.10E-01	7.43E-01	6.01E-01	7.14E-01		
d ¹⁵ N	vs. air	-3.69	0.35	-1.38	-1.38	-1.7	0.2	5.41	3.89
D ₃₀	vs. stochastic	17	3.43	10.92	10.25	11	15.5	1.5	3.9
1 se d ¹⁵ N		0.032	0.018	0.02	0.021	0.022	0.008	0.1	0.1
1 se D ₃₀		0.496	0.527	0.288	0.309	0.307	0.138	0.3	0.2
CO ₂		0.992	0.990	0.975	0.993	0.990	0.983	0.859	0.861
He		4.56E-05	5.00E-06	5.59E-06	4.97E-06	8.53E-06	6.54E-06	7.61E-06	1.66E-05
H ₂		1.17E-04	3.25E-04	1.40E-02	6.62E-05	7.05E-05	4.64E-03	1.24E-01	1.20E-01
Ar		2.42E-04	1.12E-04	1.24E-04	3.10E-04	4.21E-04	9.98E-05	1.52E-04	3.70E-05
O ₂		4.19E-04	1.25E-05	1.45E-04	5.28E-04	7.90E-04	4.54E-06	1.14E-05	8.93E-06
N ₂		6.70E-03	1.00E-02	1.06E-02	6.56E-03	8.94E-03	1.20E-02	1.62E-02	1.88E-02
CH ₄		6.44E-06	1.25E-06	1.20E-04	7.24E-06	9.48E-06	1.95E-05	8.88E-06	7.66E-06
He/Ar		1.89E-01	4.44E-02	4.50E-02	1.60E-02	2.03E-02	6.55E-02	5.00E-02	4.48E-01
N ₂ /He		1.47E+02	2.00E+03	1.91E+03	1.32E+03	1.05E+03	1.83E+03	2.13E+03	1.13E+03
N ₂ /Ar		2.77E+01	8.89E+01	8.58E+01	2.11E+01	2.12E+01	1.20E+02	1.07E+02	5.07E+02
O ₂ /N ₂		6.25E-02	1.25E-03	1.36E-02	8.04E-02	8.83E-02	3.80E-04	7.03E-04	4.76E-04
N ₂ /CH ₄		1.04E+03	8.00E+03	8.87E+01	9.06E+02	9.43E+02	6.14E+02	1.83E+03	2.45E+03
⁴⁰ Ar/ ³⁶ Ar					297	293		305	
³ He/ ⁴ He	(R _a)	6.44	7.15	6.96	7.15	7.15	7.56	6.99	6.99
N ₂ / ³ He		1.63E+07	2.00E+08	1.96E+08	1.32E+08	1.05E+08	1.73E+08	2.18E+08	1.16E+08
N ₂ / ³⁶ Ar		8.49E+03	2.72E+04	2.62E+04	6.47E+03	6.49E+03		3.26E+04	1.78E+05
⁴ He/ ²⁰ Ne		8.93E+00	1.90E+02	3.61E+02	1.56E+02	1.56E+02	6.66E+01	2.75E+02	2.75E+02
³ He/ ²² Ne		8.04E-04	1.90E-02	3.52E-02	1.56E-02	1.56E-02	7.05E-03	2.69E-02	2.69E-02
X value		28	596	1133	488	488	209	864	864
³ He/ ³⁶ Ar		5.20E-04	1.36E-04	1.34E-04	4.90E-05	6.20E-05		1.50E-04	
⁴ He/ ⁴⁰ Ar		1.89E-01	4.46E-02	4.51E-02	1.61E-02	2.03E-02		5.02E-02	

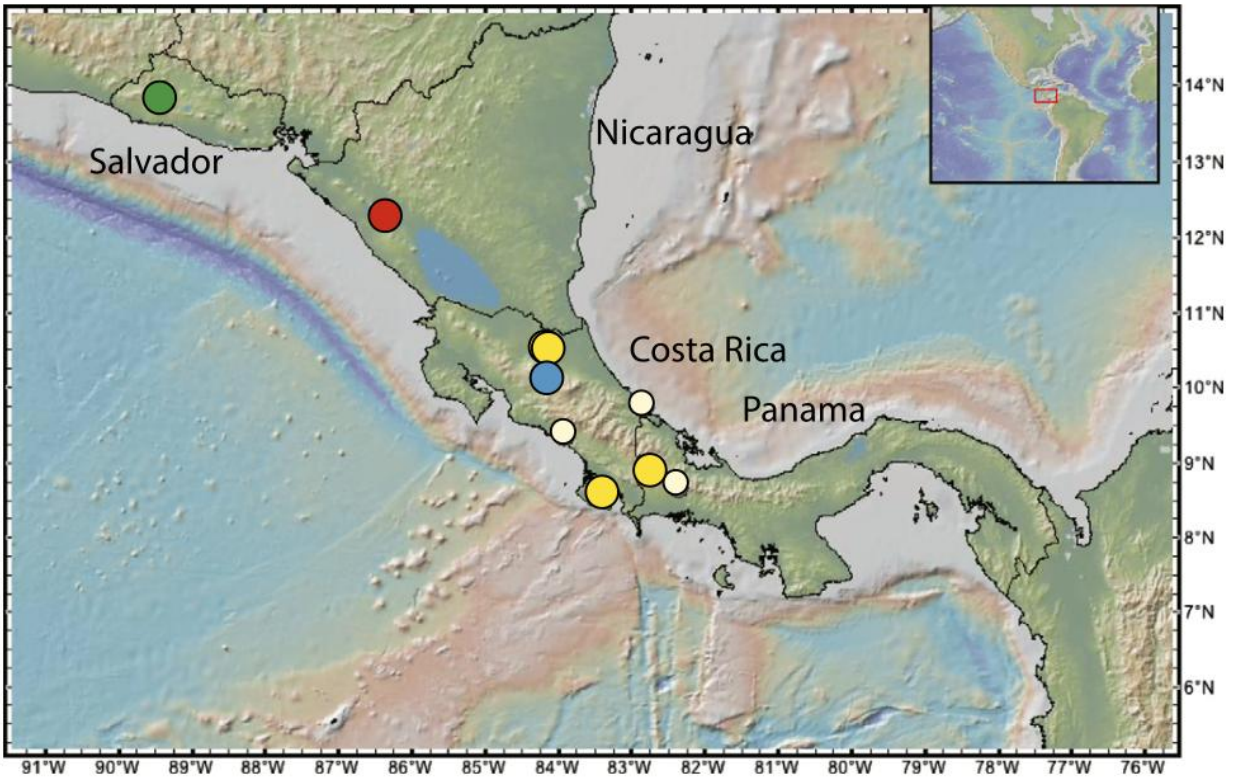
665

666 **Table 1. Nitrogen and light noble gases isotope and concentrations for central**
667 **Americans fumaroles**

668

sample ID		LH180406	CL180409	CH180410	PX180416	PS180405	BS180407	HA180403	CW180415	YF180416
spring name		Los Pozos	Colibre	Chiguiti Abajo	San Juan PraxAir	Playa Sandalo	Bajo Mended	Hatillo	Cauhita	San Juan PraxAir
latitude		8.870954	8.404478	8.705078	10.480755	8.575544	8.66645	9.360324	9.735746	10.485523
longitude		-82.689901	-80.803745	-80.269193	-84.113598	-83.36416	-82.349098	-83.916639	-82.825737	-84.113229
temperature (C)		55	51	31	29	31	41	33	35	29
quantity of processed N ₂	10 ⁶ mol	18.0	540.0	7.2	38.0	28.0	588.0	556.0	39.2	2.8
N ₂ vol fraction (ucla)	x10 ²	2.89E-02	8.67E-01	1.16E-02	6.10E-02	4.49E-02	9.44E-01	8.92E-01	6.29E-02	4.49E-03
d ¹⁵ N	vs. air	-1.38	0.55	1.60	0.20	0.71	4.19	0.22	0.34	1.30
D ₁₀	vs. stochastic	18.39	15.27	12.52	19.35	18.42	8.73	7.29	18.47	15.09
1 se d ¹⁵ N		0.029	0.004	0.028	0.007	0.008	0.004	0.004	0.004	0.031
1 se D ₁₀		0.825	0.099	0.563	0.22	0.24	0.168	0.077	0.097	0.617
CO ₂		0.997	0.018	0.985	0.944	0.082		0.031	0.054	
He		1.47E-07	4.98E-04	1.54E-05	1.97E-06	1.90E-06		4.19E-04	1.04E-05	
H ₂		9.07E-07	3.92E-06	1.77E-07	9.81E-08	1.51E-05		7.48E-05	1.62E-05	
Ar		4.79E-05	1.12E-02	3.76E-04	3.52E-04	1.07E-03		6.90E-03	1.71E-03	
O ₂		5.75E-04	4.78E-03	1.87E-03	1.19E-02	2.77E-03		3.12E-02	1.10E-02	
N ₂		2.04E-03	9.63E-01	1.32E-02	4.41E-02	5.03E-02		9.30E-01	9.92E-02	
CH ₄		9.62E-08	2.52E-03	4.53E-05	2.66E-06	8.64E-01		3.09E-04	8.34E-01	
He/Ar		3.07E-03	4.46E-02	4.09E-02	5.60E-03	1.77E-03		6.07E-02	6.09E-03	3.85E-02
N ₂ /He		1.39E+04	1.93E+03	8.54E+02	2.23E+04	2.65E+04		4.23E+04	9.56E+03	1.21E+03
N ₂ /Ar		4.27E+01	8.62E+01	3.50E+01	1.25E+02	4.69E+01		1.09E+02	1.35E+02	4.64E+01
O ₂ /N ₂		2.81E-01	4.96E-03	1.42E-01	2.69E-01	5.50E-02		3.36E-02	1.11E-01	
N ₂ /CH ₄		2.12E+04	3.83E+02	2.91E+02	1.65E+04	5.82E-02		3.01E+03	1.19E-01	
³ He	x10 ⁹ cc/ccSTP	3.21E+01	4.39E+05	1.28E+04	1.12E+03	1.65E+02		2.23E+04	3.98E+05	3.72E+03
²⁰ Ne	x10 ⁹ cc/ccSTP	2.24E+00	1.37E+04	1.23E+02	6.81E+02	3.98E+02		1.58E+04	7.07E+03	6.15E+02
⁴⁰ Ar	x10 ⁶ cc/ccSTP	3.85E+00	1.15E+04	3.59E+02	3.95E+02	4.83E+02		8.67E+03	6.35E+03	7.49E+02
³⁶ Ar	x10 ⁶ cc/ccSTP	1.28E+01	3.74E+04	1.05E+03	1.29E+03	1.59E+03		2.67E+04	2.06E+04	2.43E+03
⁴⁰ Ar/ ³⁶ Ar	(R _A)	301	308	342	305	304		325	308	309
³ He/ ⁴ He		7.48	8.78	6.37	6.52	1.55		0.27	1.82	2.05
²⁰ Ne/ ²² Ne		10.00	9.83	9.89	9.82	9.84		9.85	9.87	9.91
²¹ Ne/ ²² Ne		0.023	0.029	0.029	0.029	0.029		0.029	0.029	0.029
N ₂ / ³ He		1.33E+09	1.57E+08	9.59E+07	2.45E+09	1.22E+10		1.12E+11	8.72E+08	3.33E+09
N ₂ / ²⁰ Ne		1.29E+04	2.66E+04	1.20E+04	3.83E+04	1.43E+04		3.53E+04	4.17E+04	1.80E+04
⁴ He/ ²⁰ Ne		1.43E+01	3.21E+01	1.04E+02	1.65E+00	4.15E-01		1.41E+00	5.63E+01	7.15E+00
³ He/ ²¹ Ne		1.50E-03	3.87E-03	9.19E-03	1.48E-04	8.85E-06		5.34E-06	1.41E-03	2.02E-04
X value		45	101	327	5	1		4	177	200
³ He/ ³⁶ Ar		9.70E-06	1.69E-04	1.25E-04	1.57E-05	1.17E-06		3.16E-07	4.78E-05	5.41E-06
⁴ He/ ³⁶ Ar		3.08E-03	4.47E-02	4.10E-02	5.62E-03	1.77E-03		2.50E-03	6.09E-02	6.11E-03

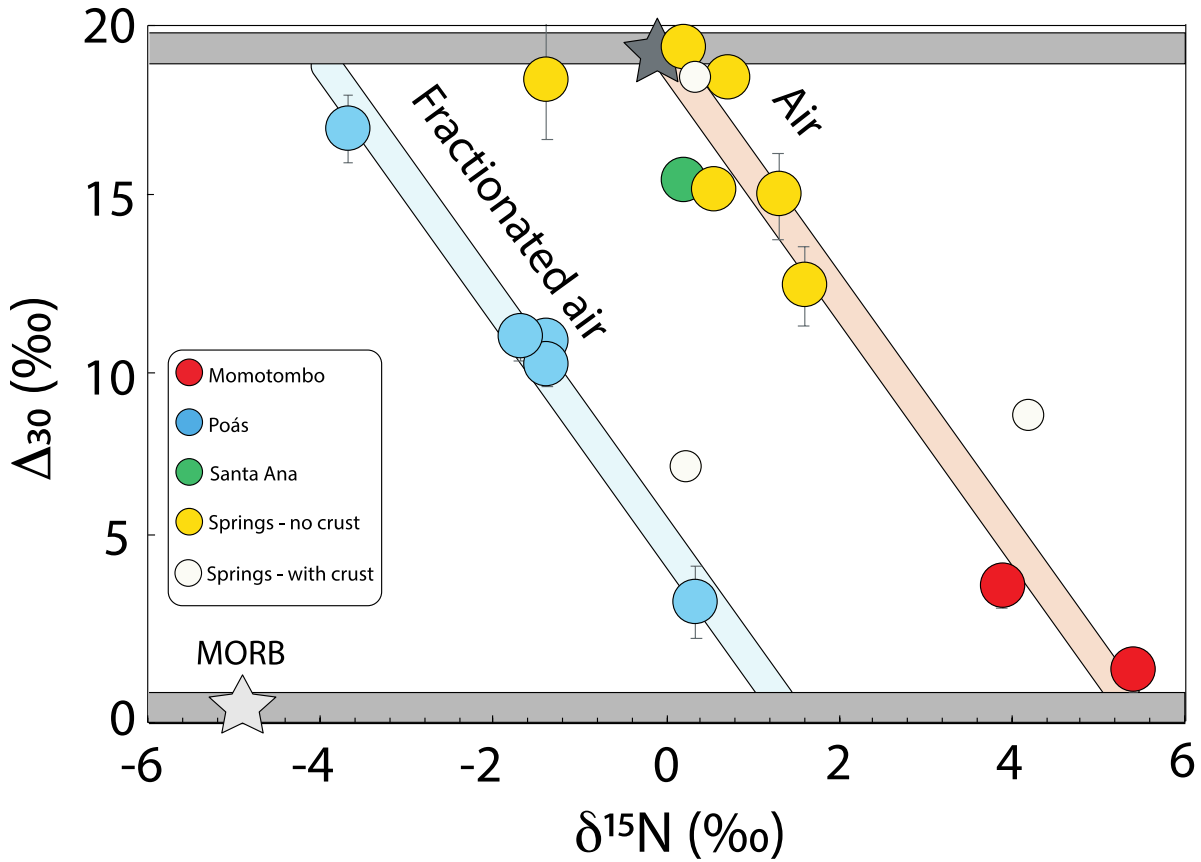
669
670 **Table 2 Nitrogen and light noble gases isotope and concentrations for central**
671 **American springs**



672

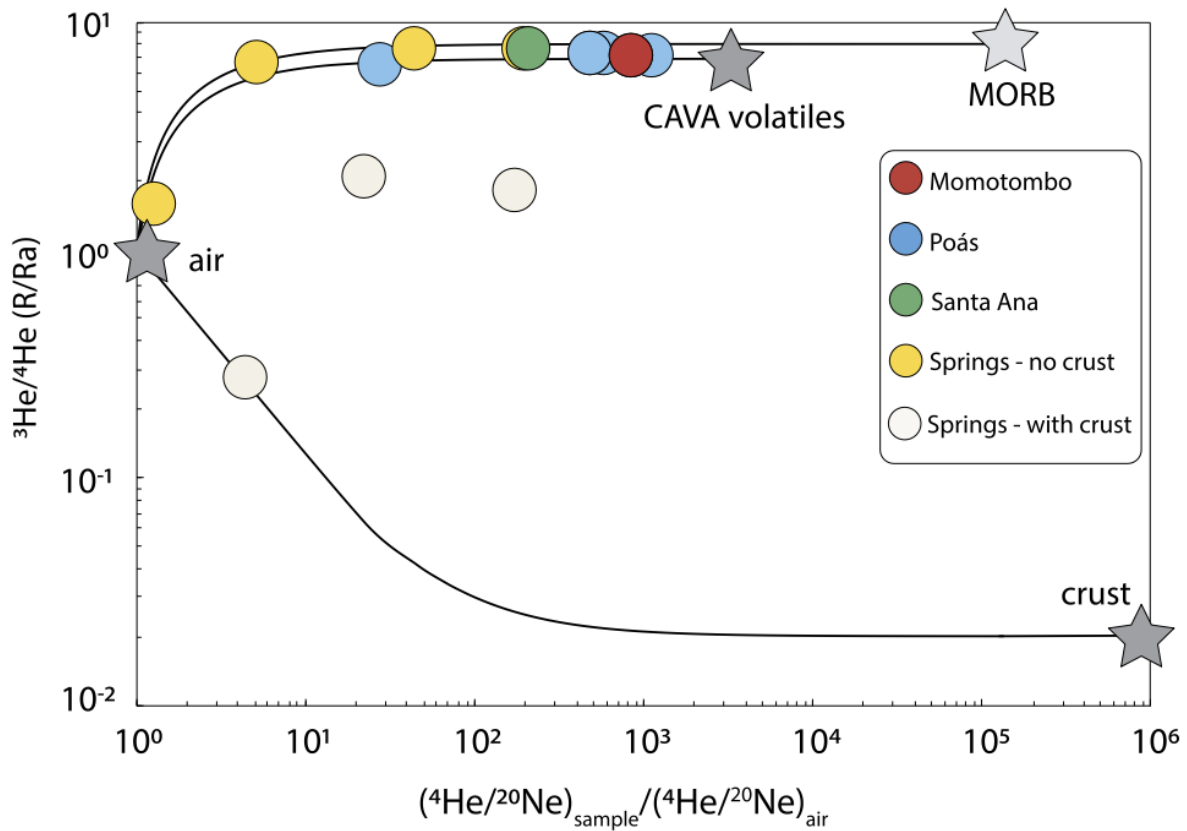
673 **Fig. 1: location of all the samples studied here.**

674 Green, red and blue symbols are fumarole locations from Santa Ana, Momotombo and Poás
 675 (Data in table 1). Yellow symbols are springs (Data in table 2).



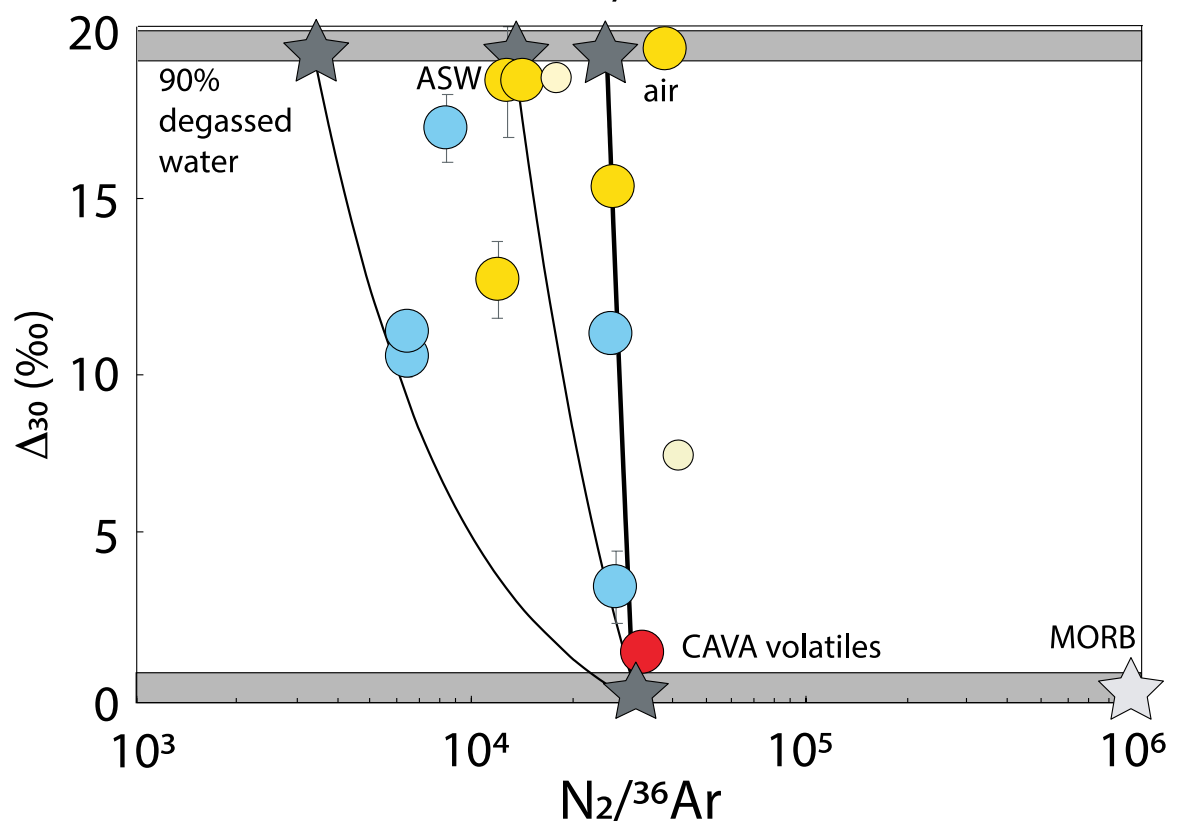
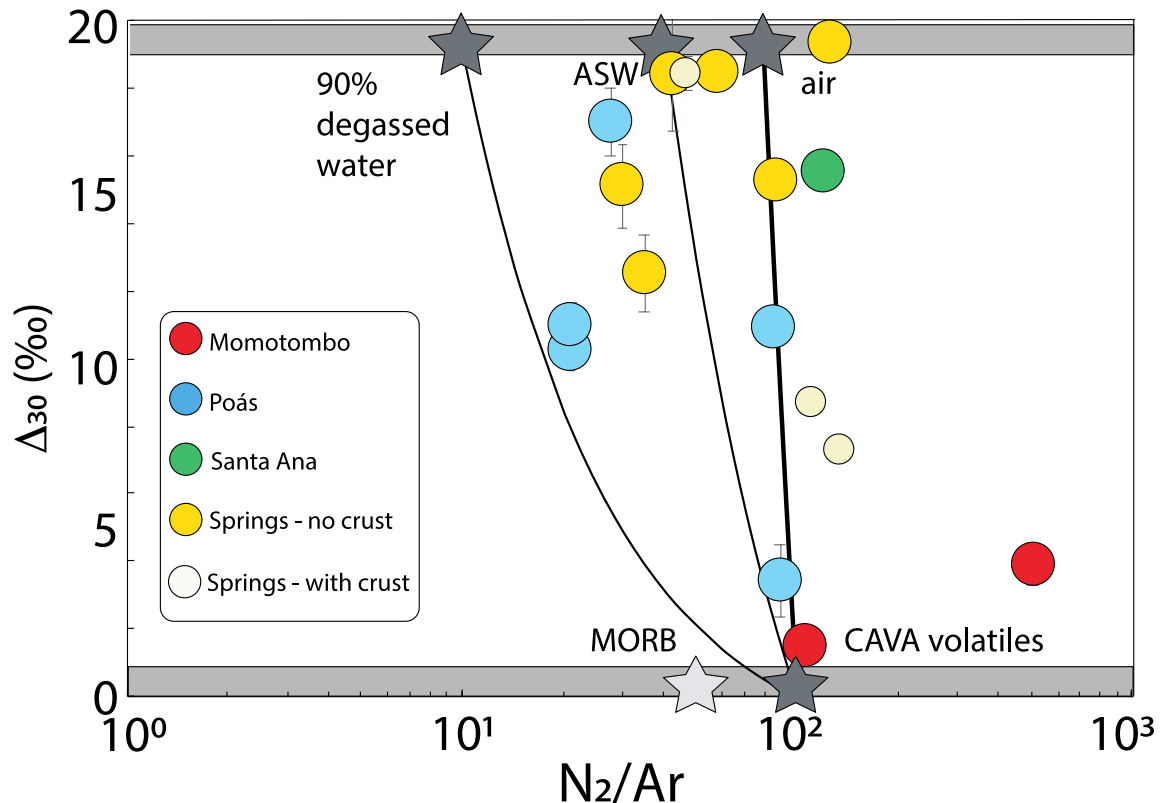
676
677

678 **Fig. 2 the nitrogen isotopic composition of volcanic discharges in central America.**
 679 Variable Δ_{30} values establish that our samples incorporate variable amounts of atmospheric
 680 nitrogen. Fumaroles from the Poás and Momotombo have the lowest Δ_{30} values indicating
 681 they have the lowest air-derived N_2 contributions while the hot springs from Costa Rica
 682 have the highest air contributions. Variable $\delta^{15}\text{N}$ values are observed, between $-3.7 \pm 0.3\text{‰}$
 683 and $+4.2 \pm 0.3\text{‰}$. At an air Δ_{30} values, variable $\delta^{15}\text{N}$ must be caused by a mass-dependent
 684 isotope fractionation, presumably associated with hydrothermal degassing. The high-
 685 temperature components have positive $\delta^{15}\text{N}$ values.

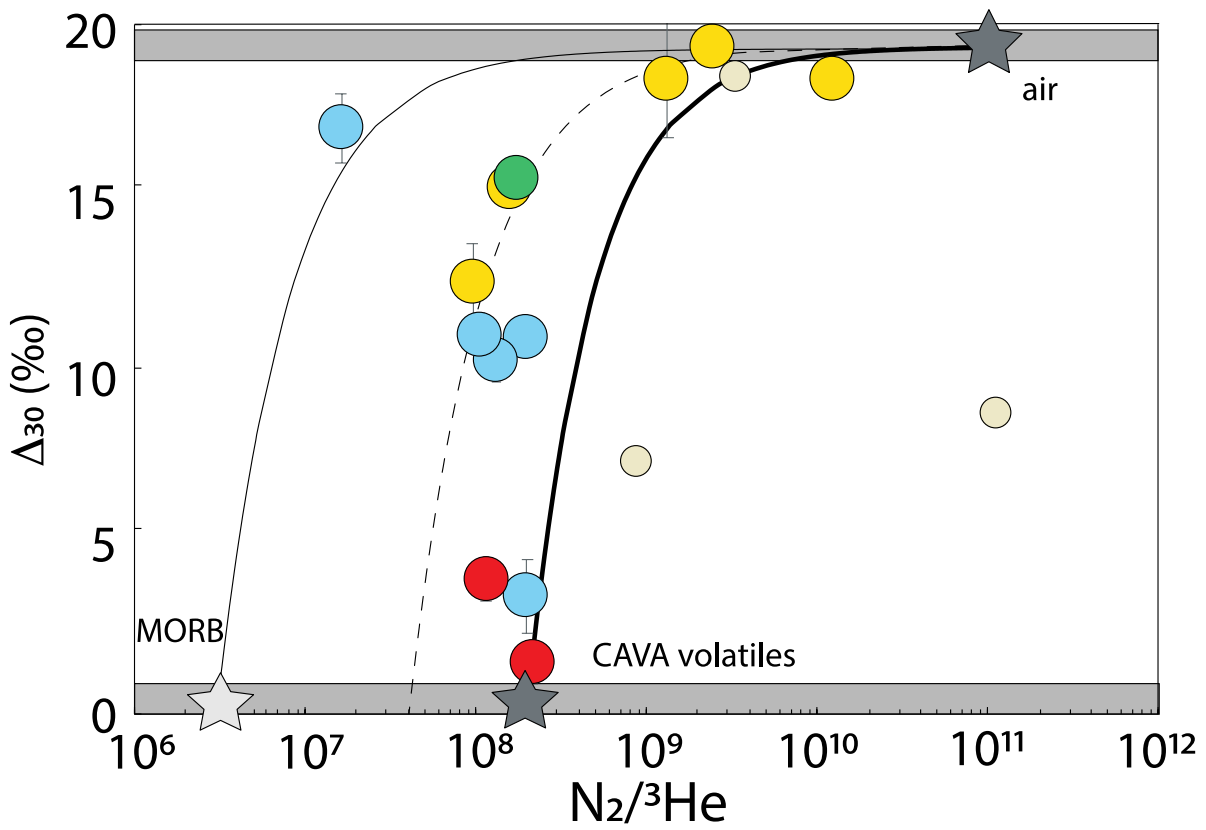
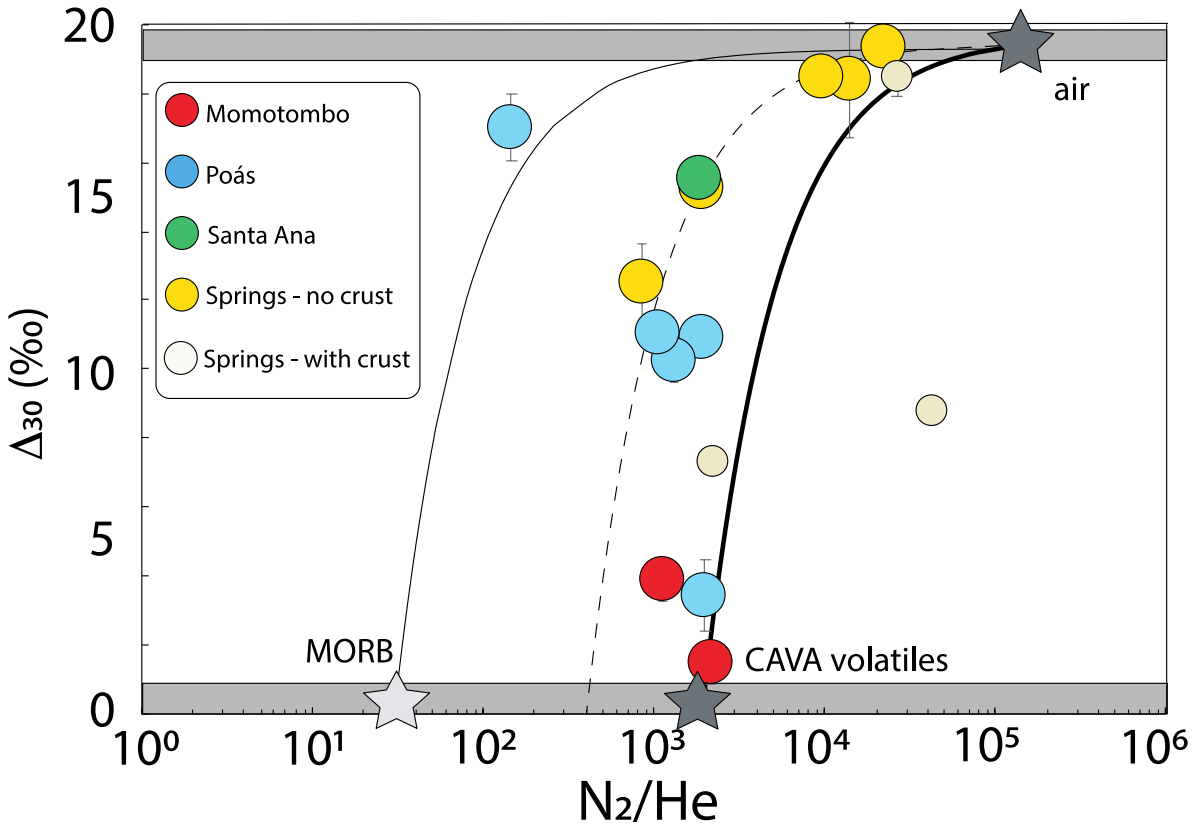


686

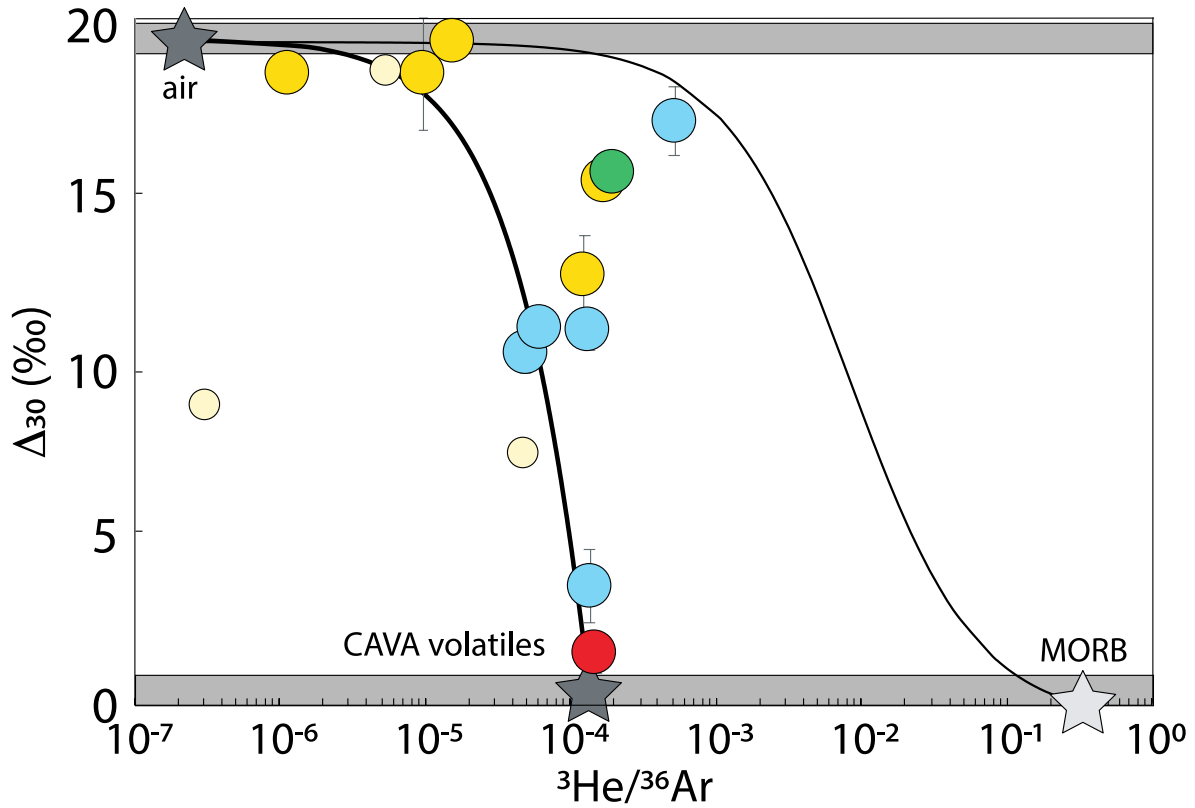
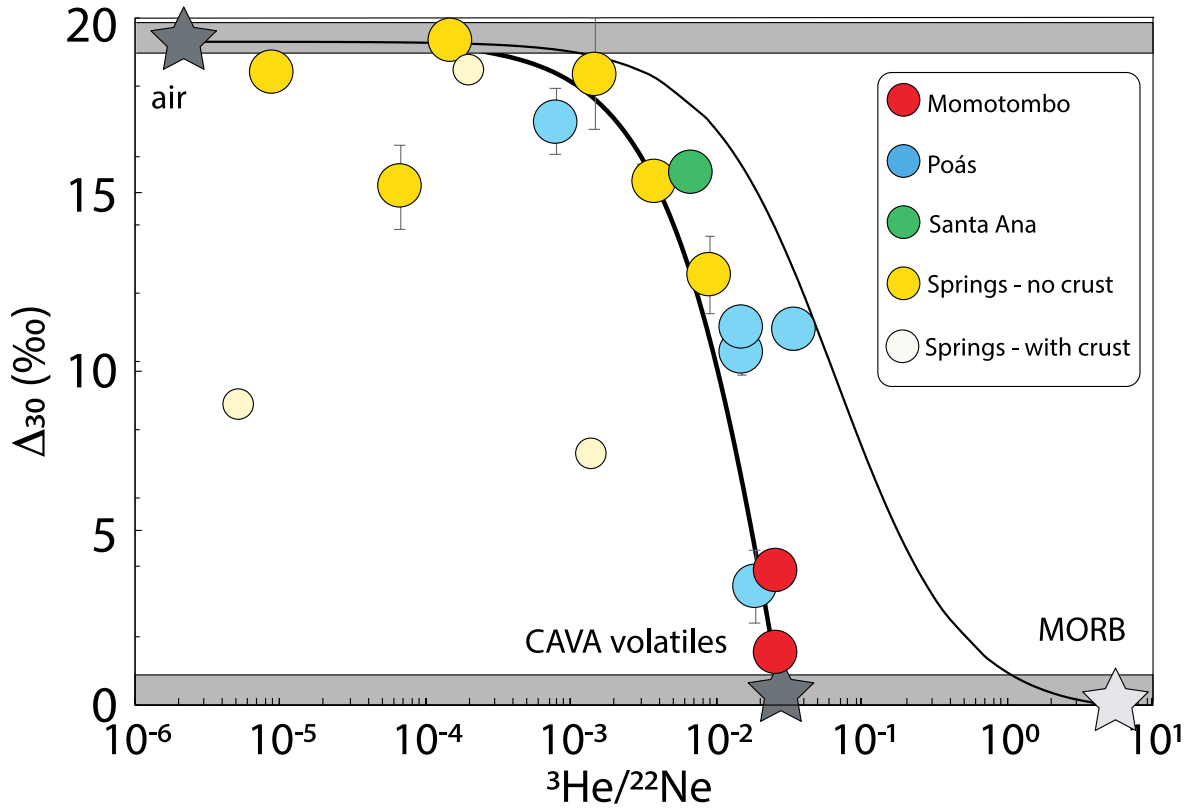
687 **Fig. 3: Measured $^3\text{He}/^4\text{He}$ ratios versus $^4\text{He}/^{20}\text{Ne}$ ratios of the samples, normalized to air by**
 688 **convention (De Leeuw et al, 2007).** Most samples indicate simple two-component air-magma
 689 mixing. Three Costa Rica hot springs (HS) however show additions of crustal ^4He .



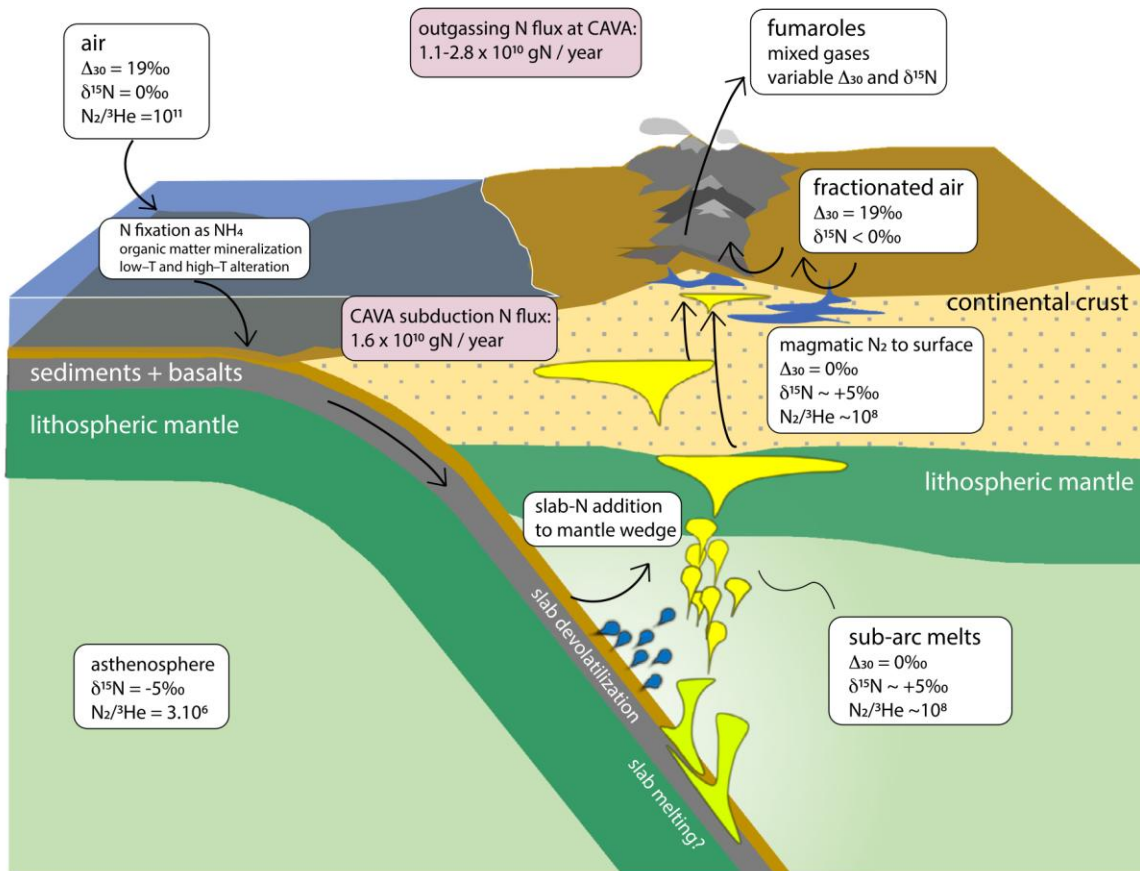
691 **Fig. 4: Measured N_2/Ar and $N_2/^{36}Ar$ ratios versus Δ_{30} values.** Mixing lines are shown for
692 mixtures between the high-temperature component observed at both Momotombo and Poás,
693 and variably fractionated atmospheric components, including air, air-saturated water (ASW),
694 and degassed water. The high-temperature endmembers with $\Delta_{30} = 0\text{‰}$ defined by the data
695 from Momotombo and Poás have similar N_2/Ar and $N_2/^{36}Ar$ ratios of ~ 100 and $\sim 10^4$,
696 respectively. Here, we adopt values of ~ 100 and 3×10^4 for N_2/Ar and $N_2/^{36}Ar$ ratios for
697 the high-T endmember at Momotombo. Nitrogen and argon have indistinguishable
698 solubilities in silicate melts and thus are not fractionated by magmatic degassing at ~ 1200
699 $^{\circ}C$ (Libourel et al., 2003). Thus, the low $N_2/^{36}Ar$ at Momotombo is not resulting from
700 fractionations during magmatic degassing. Instead, it may be a feature of the Momotombo
701 mantle source. At Poás, fumarole samples are consistent with the same N_2/Ar ratio for the
702 high-temperature component as at Momotombo. If hydrothermal degassing affected the
703 high-T volatiles at Poás, the pristine N_2/Ar and $N_2/^{36}Ar$ for high-T gases at Poás could be
704 higher than the observed values. Note that combining a $^3He/^{36}Ar$ ratio of $\sim 10^{-4}$ (see Fig.
705 6B) to the observed $N_2/^{36}Ar$ of $\sim 10^8$ (Fig. 4) returns to a $N_2/^{36}Ar$ of $\sim 10^4$, consistent with
706 the conclusion of a low N_2/Ar in our sampling of high-temperature endmembers (see
707 section 5.4).
708



710 **Fig. 5: Measured N_2/He and $N_2/^3He$ ratios versus Δ_{30} values.** Mixing lines are shown for
711 mixtures between air and three high-temperature components: MORBs, and two variably N_2 -
712 enriched endmembers required to fit the data. Springs with additions of crustal 4He are shown
713 in the smallest symbols. They are not used for fluxes calculations – see discussion in the
714 supplementary discussion.



716 **Fig. 6: Measured $^3\text{He}/^{22}\text{Ne}$ and $^3\text{He}/^{36}\text{Ar}$ ratios versus Δ_{30} values.** Springs with additions of
 717 crustal ^4He are shown in the smallest symbols. They are not used for fluxes calculations – see
 718 discussion in the supplementary discussion. Mixing lines are the same as in figure 3 and 4. They
 719 are shown for mixtures between air and high-temperature components: MORB, and a N_2 - ^{36}Ar -
 720 ^{22}Ne enriched endmember that fits the data. The mixing relationships are curved because of the
 721 logarithm scale, but also because of how distinct the N_2/Ne of the mixing endmembers may be.
 722 Air has a $\text{N}_2/^{20}\text{Ne}$ ratio of air is 4.5×10^4 . For MORB, we calculate a the $\text{N}_2/^{20}\text{Ne}$ of 1.3×10^6 . This
 723 is based on a $\text{N}_2/^3\text{He}$ of 3×10^6 for the MORB mantle (Javoy and Pineau, 1991). We combine this
 724 $\text{N}_2/^3\text{He}$ estimate with $^3\text{He}/^4\text{He}$ and $^4\text{He}/^{20}\text{Ne}$ values for the MORB mantle from Moreira et al
 725 (1998). Using the $^3\text{He}/^{22}\text{Ne}$ ratio of the MORB mantle (Moreira et al., 1998), we derive a
 726 $\text{N}_2/^{22}\text{Ne}$ of 1.7×10^7 . Conversely, we here derive $\text{N}_2/^3\text{He}$, $^3\text{He}/^{22}\text{Ne}$ ratios of the central
 727 American high-temperature volatiles. Combining those with $^3\text{He}/^4\text{He}$ of ~ 7 from Fig. 3, we
 728 derive $\text{N}_2/^{20}\text{Ne}$ and $\text{N}_2/^{22}\text{Ne}$ ratios of 3.4×10^5 and 3.3×10^6 , respectively. On panel b, the
 729 curvatures are function the N_2/Ar of the mixing endmembers, which are estimated on Fig. 4.
 730



731
 732 **Fig. 7 Cartoon representing various processes and reservoirs constrained in this study.** Scales
 733 are grossly exaggerated, especially for melt conduits and magma chambers. A slab with
 734 sediments, basalts, and oceanic lithospheric mantle is shown to enter subduction. The slab
 735 composition is not constrained here but is likely enriched in all volatiles relative to ^3He (Busigny
 736 et al., 2019, Chavrit et al., 2016). In the slab, nitrogen is fixed as NH_4^+ (Busigny et al., 2019 and

737 references therein) so no Δ_{30} values are defined; Δ_{30} is only relevant for N₂ molecules. Both slab
738 devolatilization and slab melting are shown for illustration. Any slab melting would be relevant
739 underneath Costa Rica (Hoernle et al., 2008) while slab devolatilization and sediment-derived
740 fluids would contribute to sources underneath Nicaragua and El Salvador (Patino et al., 2000).
741 The melting region is characterized as the high-temperature endmembers constrained in this
742 work (Fig. 7). Melts and super-critical fluids are suggested to host dissolved N₂ (Libourel et al.,
743 2003; Mikhail and Sverjensky, 2014). Upon partial melting of a NH₃-bearing mantle source,
744 magmatic N₂ would form with a Δ_{30} of 0‰. The high-T N₂ is then contributed to hydrothermal
745 systems in the sub-surface by near-quantitative magmatic degassing. Air circulation in the sub-
746 surface allows air-saturated waters to undergo degassing, and subsequent gas release with
747 fractionated compositions.

748

749